Theory of nonequilibrium asymptotic state thermodynamics: Interacting Ehrenfest urn ring as an example

Chi-Ho Cheng (鄭智豪) [1,*] and Pik-Yin Lai (黎璧賢)[2,3,†]

[1]*Department of Physics, National Changhua University of Education, Taiwan, Republic of China*
[2]*Department of Physics and Center for Complex Systems, National Central University, Taiwan, Republic of China*
[3]*Physics Division, National Center for Theoretical Sciences, Taipei 10617, Taiwan, Republic of China*

A generalized class of the nonequilibrium state, called the nonequilibrium asymptotic state (NEAS), is proposed. The NEAS is constructed within the framework of Fokker-Planck equations in thermodynamic limit. Besides the usual equilibrium state and nonequilibrium steady state (NESS), the class of NEAS could also cover the nonequilibrium periodic state (NEPS) in which its dynamics shows periodicity, the nonequilibrium quasiperiodic state (NEQPS), and nonequilibrium chaotic state (NECS) in which its dynamics becomes chaotic. Based on the theory of NEAS thermodynamics, the corresponding thermodynamics of different NEASs could also be determined. Finally the interacting Ehrenfest urn ring model is used as an example to illustrate how different kinds of NEAS (equilibrium state, uniform NESS, nonuniform NESS, NEPS) in the three-urn case are identified in our framework. In particular, the thermodynamics of NEPS and its phase transitions to other types of NEAS are studied.

DOI: 10.1103/PhysRevE.108.064114

I. INTRODUCTION

In nature, equilibrium physics are widely studied, but nonequilibrium phenomena often occur. The appearance of nonequilibrium may not be due to imperfect environment or by accident. In some cases, nonequilibrium phenomena appear for the sake of some functionality, especially just after breaking the detailed balance. For example, in a recent study, it was found that detailed balance violations in the brain increase with physical and cognitive exertion [1].

Near equilibrium, linear response theory provides a way to calculate the nonequilibrium properties from the correlation functions at equilibrium. Beyond the linear response regime, in small systems, fruitful results were obtained from the realm of stochastic thermodynamics in which the thermodynamic quantities like heat transfer, external work done, and entropy production are defined along individual trajectories and also their relationship can be identified [2–6]. The fluctuation theorem was initally discovered in nonequilibrium steady states [7], and later proved in other nonequilibrium situations [8–10]. By relating the free-energy difference between two equilibrium states through the nonequilibrium process with work done, the Jarzynski relation was achieved [11,12]. Later, many variations and its realization were proposed [13–15]. If the initial and final equilibrium states are extended to nonequilibrium steady states (NESSs), the Hatano-Sasa equality can be found [16], which follows from a more general framework of steady-state thermodynamics [17,18].

Among the nonequilibrium states, the NESSs are widely studied [19–22]. In addition, the nonequilibrium nonsteady states may also induce lots of physical insight to nonequilibrium physics. For example, when the system exhibits periodic dynamics, its thermodynamics may behave differently. Recently, a model of three state interacting driven oscillators is shown to exhibit periodic dynamics. After incorporating with the stochastic thermodynamics process, a phase transition between different nonequilibrium states is illustrated [23]. Under the framework of stochastic thermodynamics, the driven Potts model also exhibits the thermodynamics of nonequilibrium nonsteady states [24]. The inclusion of noise (similar to temperature effect) into the standard Stuart-Landau dimer model [25] (its dynamics exhibits limit cycles) provides insight into the importance of coherent synchronization within the working substance in the operation of a thermal machine.

Even in the quantum case, limit cycles induced by periodically driven quantum thermal machines may provide insights towards the development of quantum thermodynamics [26–32].

Throughout the above studies, there is a lack of formulation to merge dynamics and thermodynamics in a natural way. Within this formulation, in the thermodynamic limit, macroscopic quantities and thermodynamic phenomena like phase transitions can be well-defined and studied. Their dynamics and thermodynamics would not be independent but mutually affected. Our approach based on the Fokker-Planck equation is particularly advantageous to handle systems in the thermodynamic limit (large N limit) over other approaches. This is the scope of the current paper.

The content is organized as follows. In Sec. II, we first develop a formalism (large number of degree of freedom) to study the asymptotic behavior of the thermodynamic state,

*phcch@cc.ncue.edu.tw
†pylai@phy.ncu.edu.tw

namely, the nonequilibrium asymptotic state (NEAS). Within the framework, NEAS is identified as a WKB solution which covers the equilibrium state; NESS; nonequilibrium periodic state (NEPS), in which its dynamics shows periodicity (limit cycles); and even the nonequilibrium chaotic state (NECS), in which its dynamics becomes chaotic. Then, in Sec. III, the Ehrenfest urn ring model [33,34] is introduced as an example to illustrate the NEAS. In particular, in Sec. IV, when the number of urns is restricted to three, the behaviors of different kinds of NEASs [equilibrium state, uniform NESS (uNESS), nonuniform NESS (nuNESS), and NEPS] and their phase transitions are demonstrated. In Sec. V, the thermodynamic fluctuation effect is retrieved from the fluctuation around the WKB solution to the Fokker-Planck equation. A thermodynamic relation is then identified. To characterize the nature of phase transition, a correspondence between dynamical and thermodynamic characterization is found. Further, it can also be proved that the dynamical stability criteria implies the thermodynamic stability. Incidentally, both criteria are equivalent in the NESS of the Ehrenfest ring model. Finally, the conclusion is presented in Sec. VI.

II. FORMALISM OF NONEQUILIBRIUM ASYMPTOTIC STATES

In this section, we show how one extends the concept of NESS to NEAS. The framework for NEAS also holds for NESS, i.e., NESS is just a special case in the NEAS formalism.

Suppose we consider the Fokker-Planck equation of dimension D of the following form:

$$
\frac{\partial \rho(\vec{x}, t)}{\partial t} = -\sum_{i=1}^{D} \frac{\partial}{\partial x_i}[A_i(\vec{x}, t)\rho(\vec{x}, t)]
$$
$$
+ \frac{1}{2N} \sum_{i,j=1}^{D} \frac{\partial^2}{\partial x_i \partial x_j}[B_{ij}(\vec{x}, t)\rho(\vec{x}, t)], \quad (1)
$$

where $\rho(\vec{x}, t)$ is the probability density of state $\vec{x}$ in our system. $A_i(\vec{x}, t) \equiv \lim_{\tau \to 0} \frac{1}{\tau} \int d^D x'(x'_i - x_i)W(\vec{x}', t + \tau | \vec{x}, t)$ and $B_{ij}(\vec{x}, t) \equiv N \lim_{\tau \to 0} \frac{1}{\tau} \int d^D x'(x'_i - x_i)(x'_j - x_j)W(\vec{x}', t + \tau | \vec{x}, t)$, with the transition probability $W(\vec{x}', t + \tau | \vec{x}, t)$ from state $\vec{x}$ at time t to state $\vec{x}'$ at time $t + \tau$. N is a large number proportional to the system's degrees of freedom. (For example, in a system of many particles, N refers to the total particle number.) $A_i(\vec{x}, t)$ and $B_{ij}(\vec{x}, t)$ are functions of $O(1)$. Equation (1) is a general equation describing the evolution of the probability density in the large N limit, which can be derived from the general master equation as outlined in Ref. [34]. In the large N limit (thermodynamic limit), the WKB ansatz could be applied [35], which reads

$$
\rho(\vec{x}, t) \propto e^{Nf}, \quad (2)
$$

where f is a function of $O(1)$. The traditional WKB method takes $f = f(\vec{x})$, which means to assume that the final state is a steady state. It is beyond the scope of the method if the steady state is not favorable (to nonsteady states) or doesn't even exist. Hence, we extend $f = f(\vec{x})$ to $f = f(\vec{x}, t)$ so

the steady and nonsteady states are both considered. Further, there exists a time-dependent optimal point [36] $\vec{\xi}(t)$ such that $\partial_i f(\vec{\xi}(t), t) = 0$ (its stability could be justified later). Hence one can expand $f(\vec{x}, t)$ around $\vec{x} = \vec{\xi}(t)$, i.e., $f(\vec{x}, t) \simeq f(\vec{\xi}(t), t) + \frac{1}{2} \sum_{ij} \partial_{ij} f(\vec{\xi}(t), t)(x_i - \xi_i(t))(x_j - \xi_j(t))$, so Eq. (2) can be rewritten as

$$
\rho(\vec{x}, t) \propto \exp\left[N \sum_{i,j=1}^{D} c_{ij}(t)(x_i - \xi_i(t))(x_j - \xi_j(t)) \right] \quad (3)
$$

up to the leading order in N, and $c_{ij}(t) \equiv \frac{1}{2} \partial_{ij} f(\vec{\xi}(t), t)$. Obviously the matrix $\mathbf{c}$ is symmetric by its definition.

The form of Eq. (3) implies the main contribution of probability density from the neighborhood of $\vec{x} = \vec{\xi}(t)$ in the large N limit. We can then further simplify Eq. (1) by expanding $A_i(\vec{x}, t) \simeq A_i(\vec{\xi}(t), t) + \sum_j \partial_j A_i(\vec{\xi}(t), t)(x_j - \xi_j(t)) \equiv A_i(\vec{\xi}(t), t) + \sum_j a_{ij}(t)(x_j - \xi_j(t))$, and $B_{ij}(\vec{x}, t) \simeq B_{ij}(\vec{\xi}(t), t) \equiv b_{ij}(t)$. Under this approximation, Eq. (1) becomes

$$
\frac{\partial \rho(\vec{x}, t)}{\partial t}
$$
$$
= -\sum_{i=1}^{D} \frac{\partial}{\partial x_i} \left[\left(A_i(\vec{\xi}(t), t) + \sum_{j=1}^{D} a_{ij}(t)(x_j - \xi_j(t)) \right) \rho(\vec{x}, t) \right]
$$
$$
+ \frac{1}{2N} \sum_{i,j=1}^{D} b_{ij}(t) \frac{\partial^2}{\partial x_i \partial x_j} \rho(\vec{x}, t). \quad (4)
$$

Substitution of Eq. (3) into the above equation and keeping the leading order in N (see Appendix A for details) gives

$$
\partial_t \vec{\xi} = \vec{A}(\vec{\xi}, t), \quad (5)
$$

$$
\partial_t \mathbf{c}^{-1} = \mathbf{a}\mathbf{c}^{-1} + \mathbf{c}^{-1}\mathbf{a}^t - 2\mathbf{b}. \quad (6)
$$

Equation (5) is the dynamical equation to describe the state evolution. The asymptotic behavior of the dynamical state [here we call it $\vec{\xi}^{\text{as}}(t)$] could be fixed points ($\partial_t \vec{\xi}^{\text{as}} = 0$), limit cycles [$\vec{\xi}^{\text{as}}(t)$ follows some kind of periodic trajectory], quasiperiodic, or even chaotic states [37].

After incorporating with thermal fluctuations from Eq. (6), the thermodynamic states are then classified into the equilibrium state (dynamical fixed point with detailed balance), NESS (dynamical fixed point with detailed balance violation), NEPS (dynamical limit cycles), nonequilibrium quasiperiodic state (NEQPS), and NECS. All the above thermodynamic states are the possible NEAS, from which we define the asymptotic behavior of Eqs. (5) and (6) in the framework under Eq. (1) with WKB ansatz in Eq. (2).

For the NESS, there are two stability criteria. One is the dynamical stability derived from Eq. (5), saying that the real part of all eigenvalues of $\mathbf{a}$ is negative. The other is the thermodynamic stability which is justified by its (thermodynamic) fluctuation $\mathbf{c}$, in which its time evolution is described in Eq. (6). In particular, at the NESS which corresponds to fixed point $\partial_t \vec{\xi} = 0$, $\mathbf{c}$ is time independent. From Eq. (6), $\partial_t \mathbf{c} = 0$ leads to the Lyapunov equation $\mathbf{a}\mathbf{c}^{-1} + \mathbf{c}^{-1}\mathbf{a}^t = 2\mathbf{b}$ (please refer to Appendix A in Ref. [34] for details). If further
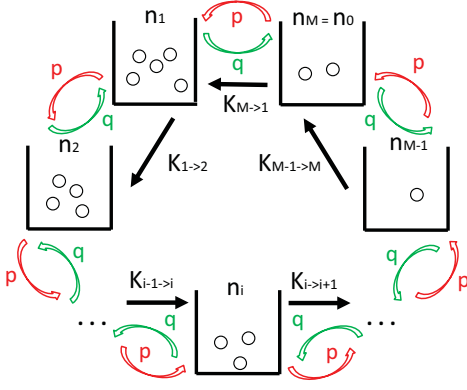
FIG. 1. Schematic diagram of the interacting Ehrenfest urn ring model. M urns with particle numbers n_i in the ith urn are connected in a ring. For convenience, we label $n_0 \equiv n_M$. The direct jumping rate in anticlockwise (clockwise) direction is p (q). $K_{i \to j}$ represents net particle flow rate from the ith to the jth urn.

at equilibrium, the detailed balance condition ($\mathbf{ab} = \mathbf{ba}^t$) is satisfied, $\mathbf{c} = \mathbf{b}^{-1}\mathbf{a}$ (please refer to Appendix B in Ref. [34] for details). The NESS stability condition is that all eigenvalues of $\mathbf{c}$ are negative. It can be proved that, for the NESS, the thermodynamic stability is satisfied if the system is dynamical stable (see Appendix B for the proof).

III. EHRENFEST URN RING MODEL

In this section, we applied the NEAS formalism in the previous section on the Ehrenfest urn ring model with interactions [33,34] to illustrate the NEAS thermodynamics. As shown in Fig. 1, M urns are connected in a ring. Particles in the same urn interact with each other, but no interaction between two particles from different urns. Further, a direct jumping rate along the ring is introduced such that the probability of an anticlockwise (clockwise) direction is p (q), and $p + q = 1$ is imposed for convenience.

The state of the system is labeled by the particle occupation distribution in the urn ring, $\vec{n} = (n_1, n_2, \ldots, n_M)$ where n_i is the particle number in the ith urn with fixed total particle number N, i.e., $\sum_{i=1}^{M} n_i = N$. For convenience, we also define $n_0 \equiv n_M$ (periodic boundary conditions). At each step, the transition probability from state $\vec{n}$ to state $\vec{m}$ is

$$T_{\vec{m}, \vec{n}} = \frac{1}{e^{-\frac{g}{N}(n_i - n_j - 1)} + 1}, \tag{7}$$

where $m_i = n_i - 1$ and $m_j = n_j + 1$. $g \equiv NJ\beta$, where β is the inverse of the effective temperature (please refer to Ref. [38] for its derivation). After s steps from the initial state, the state probability $\rho(\vec{n}, s)$ satisfies the following master equation:

$$\rho(\vec{n}, s+1) - \rho(\vec{n}, s) = \sum_{\vec{m}} (W_{\vec{n}, \vec{m}} \rho(\vec{m}, s) - W_{\vec{m}, \vec{n}} \rho(\vec{n}, s)), \tag{8}$$

where the discrete transition probability from state $\vec{n}$ to state $\vec{m}$ is $W_{\vec{m}, \vec{n}} = \frac{n_i}{N} p T_{\vec{m}, \vec{n}}$ for an anticlockwise jump and $W_{\vec{m}, \vec{n}} = \frac{n_i}{N} q T_{\vec{m}, \vec{n}}$ for a clockwise jump.

Let the (physical) time $t = \frac{\tau_1}{N} s$, where τ_1 is the timescale of each single step from s to $s + 1$, and $\tau_1 \equiv 1$ in the fol-

lowing for convenience. $\vec{x} \equiv \vec{n}/N$. In the large N limit, the discrete master equation in Eq. (8) can be transformed into the Fokker-Planck equation in Eq. (1) with $D = M - 1$ after we further keep terms up to $O(1/N^2)$. The corresponding $A_i(\vec{x})$ and $B_{ij}(\vec{x})$ are

$$A_i(\vec{x}) = -\frac{px_i}{e^{-g(x_i - x_{i+1})} + 1} + \frac{qx_{i+1}}{e^{-g(x_{i+1} - x_i)} + 1} + \frac{px_{i-1}}{e^{-g(x_{i-1} - x_i)} + 1} - \frac{qx_i}{e^{-g(x_i - x_{i-1})} + 1}, \tag{9}$$

$$B_{ii}(\vec{x}) = \frac{px_i}{e^{-g(x_i - x_{i+1})+1}} + \frac{qx_{i+1}}{e^{-g(x_{i+1} - x_i)} + 1} + \frac{px_{i-1}}{e^{-g(x_{i-1} - x_i)} + 1} + \frac{qx_i}{e^{-g(x_i - x_{i-1})} + 1}, \tag{10}$$

$$B_{i,i+1}(\vec{x}) = B_{i+1,i}(\vec{x})$$
$$= -\frac{px_i}{e^{-g(x_i - x_{i+1})} + 1} - \frac{qx_{i+1}}{e^{-g(x_{i+1} - x_i)} + 1}, \tag{11}$$

which do not have explicit time dependence, i.e., the system is autonomous with $\vec{A} = \vec{A}(\vec{\xi}(t))$ in Eq. (5). Note that the dimension of the state $\vec{x}$ in the probability density $\rho(\vec{x}, t)$ is reduced to $M - 1$ because there are only $M - 1$ independent variables due to the constraint $\sum_{i=1}^{M} x_i = 1$. The population fraction of the particles are, in general, heterogeneous and time dependent. One can define the nonuniformity for arbitrary M urns [34],

$$\psi(t) \equiv \frac{1}{M(M-1)} \sum_{(i<j)=1}^{M} \langle (x_i - x_j)^2 \rangle, \tag{12}$$

which can also reflect to some extent the orderliness of the nonequilibrium state.

A. Nonequilibrium thermodynamic relation

We identified the thermodynamic relation relating the entropy production ($\frac{dS}{dt}$) and internal entropy production ($\frac{d_iS}{dt}$) rates to the work ($\frac{dW}{dt}$) and energy ($\frac{dE}{dt}$) rates of the system,

$$\frac{dS}{dt} = \frac{d_iS}{dt} + \beta \frac{dE}{dt} + \beta \frac{dW}{dt}, \tag{13}$$

which is proved to be valid for the M-urn ring model in Appendix D for general nonequilibrium processes (asymptotic or nonasymptotic states). The thermodynamic relation has been verified in the NESS for the three-urn model in Ref. [34], and the relevant energetic quantities of the NEPS in the M-urn ring will be calculated below.

B. Energetics of NESS and NEPS in the M-urn ring

When the system is at the NEPS, suppose the oscillation period is T. Consider the cyclic permutation symmetry of M urns in a ring, and then expand $\vec{\xi}^{ps}(t)$ in Fourier series in time, which gives

$$\xi_i^{ps}(t) = \frac{1}{M} + \sum_{k=1}^{\infty} c_k \cos\left(\frac{2k\pi}{T} t - (i-1)\frac{2\pi}{M}\right), \tag{14}$$

where the coefficients c_k depend on g and p.

The (Boltzmann) entropy S^{ps} and the system energy βE^{ps} are given by

$$S^{\mathrm{ps}} \equiv -\int d^{M-1}x \rho^{\mathrm{ps}}(\vec{x},t) \ln\left(\rho^{\mathrm{ps}}(\vec{x},t)/\frac{N!}{\prod_{i=1}^{M} n_i!}\right)$$

$$= -N \sum_{i=1}^{M} \xi_i^{\mathrm{ps}}(t) \ln \xi_i^{\mathrm{ps}}(t) + O(1), \qquad (15)$$

The base of logarithms throughout the paper is e, and hence log means natural log.

$$\beta E^{\mathrm{ps}} \equiv \int d^{M-1}x \rho^{\mathrm{ps}}(\vec{x},t) \frac{g}{2} \sum_{i=1}^{M} n_i(n_i-1)$$

$$= \frac{Ng}{2} \sum_{i=1}^{M} \left(\xi_i^{\mathrm{ps}}(t)\right)^2 + O(1). \qquad (16)$$

Their rates of change are then

$$\frac{dS}{dt}\bigg|_{\mathrm{ps}} = -N \sum_{i=1}^{M} \left(\ln \xi_i^{\mathrm{ps}}(t) + 1\right) A_i(\vec{\xi}^{\mathrm{ps}}(t)), \qquad (17)$$

$$\beta \frac{dE}{dt}\bigg|_{\mathrm{ps}} = Ng \sum_{i=1}^{M} \xi_i^{\mathrm{ps}}(t) A_i(\vec{\xi}^{\mathrm{ps}}(t)). \qquad (18)$$

The rate of work done by the system is

$$\beta \frac{dW}{dt}\bigg|_{\mathrm{ps}} \equiv -N \sum_{\vec{n}} \left\{ \sum_{\vec{m}}^{\mathrm{ac}} W_{\vec{m},\vec{n}} \rho^{\mathrm{ps}}(\vec{n},t) \ln\left(\frac{p}{q}\right) \right.$$

$$\left. + \sum_{\vec{m}}^{\mathrm{c}} W_{\vec{n},\vec{m}} \rho^{\mathrm{ps}}(\vec{m},t) \ln\left(\frac{q}{p}\right) \right\}$$

$$= -\beta N\mu \sum_{\vec{n}} \sum_{\vec{m}}^{\mathrm{ac}} (W_{\vec{m},\vec{n}} \rho^{\mathrm{ps}}(\vec{n},t) - W_{\vec{n},\vec{m}} \rho^{\mathrm{ps}}(\vec{m},t))$$

$$= -\beta\mu \sum_{i=0}^{M-1} K_{i \to i+1}^{\mathrm{ps}}(t), \qquad (19)$$

where ac (c) stands for the anticlockwise (clockwise) direction. $\mu \equiv \beta^{-1} \ln(\frac{p}{q})$ is the effective chemical potential difference to actively drive the particle from the ith to the $(i+1)$th urn. $K_{i \to i+1}^{\mathrm{ps}}(t)$ is the net particle flow rate from the ith to the $(i+1)$th urn at NEPS, defined as

$$K_{i \to i+1}^{\mathrm{ps}}(t) \equiv N \sum_{\vec{n}} (W_{(n_i-1,n_{i+1}+1),(n_i,n_{i+1})}$$

$$- W_{(n_i+1,n_{i+1}-1),(n_i,n_{i+1})}) \rho^{\mathrm{ps}}(\vec{n},t)$$

$$= N \frac{p\xi_i^{\mathrm{ps}}(t) e^{g\xi_i^{\mathrm{ps}}(t)} - q\xi_{i+1}^{\mathrm{ps}}(t) e^{g\xi_{i+1}^{\mathrm{ps}}(t)}}{e^{g\xi_i^{\mathrm{ps}}(t)} + e^{g\xi_{i+1}^{\mathrm{ps}}(t)}} + O(1). \qquad (20)$$

At NEPS, $\frac{dS}{dt}|_{\mathrm{ps}}$ and $\beta\frac{dE}{dt}|_{\mathrm{ps}}$ do not vanish, in general. However, their time average $\langle\ldots\rangle_t$ over a period T should be zero because both S^{ps} and E^{ps} are functionals of $\vec{\xi}^{\mathrm{ps}}(t)$ which is periodic:

$$\left\langle \frac{dS}{dt}\bigg|_{\mathrm{ps}} \right\rangle_t = \frac{1}{T} \int_0^T dt \frac{dS}{dt}\bigg|_{\mathrm{ps}}$$

$$= \frac{1}{T}(S(\vec{\xi}^{\mathrm{ps}}(T)) - S(\vec{\xi}^{\mathrm{ps}}(0))) = 0. \qquad (21)$$

The same argument also applies to E^{ps}, so $\langle\frac{dE}{dt}|_{\mathrm{ps}}\rangle_t = 0$. According to the thermodynamic law (see Appendix D), $dS = d_iS + \beta dE + \beta dW$, we then arrive at a generalized relationship at the NEAS:

$$\left\langle \frac{d_iS}{dt}\bigg|_{\mathrm{as}} \right\rangle_t = -\beta \left\langle \frac{dW}{dt}\bigg|_{\mathrm{as}} \right\rangle_t. \qquad (22)$$

From Eq. (19),

$$\beta \left\langle \frac{dW}{dt}\bigg|_{\mathrm{ps}} \right\rangle_t = -\beta\mu \sum_{i=0}^{M-1} \langle K_{i \to i+1}^{\mathrm{ps}}(t)\rangle_t. \qquad (23)$$

From the dynamical equation in Eq. (5), taking the time average:

$$\langle A_i(\vec{\xi}^{\mathrm{ps}}(t))\rangle_t = \frac{1}{T} \int_0^T dt \,\partial_t \xi_i^{\mathrm{ps}}(t) = 0. \qquad (24)$$

Note from Eqs. (9) and (20) that $NA_i(\vec{\xi}^{\mathrm{ps}}(t)) = -K_{i \to i+1}^{\mathrm{ps}}(t) + K_{i-1 \to i}^{\mathrm{ps}}(t)$, which implies $\langle K_{i \to i+1}^{\mathrm{ps}}(t)\rangle_t$ are equal to each other for any i.

At the NEPS, let $K^{\mathrm{ps}} \equiv \langle K_{i \to i+1}^{\mathrm{ps}}(t)\rangle_t$, then

$$\left\langle \frac{d_iS}{dt}\bigg|_{\mathrm{ps}} \right\rangle_t = -\beta \left\langle \frac{dW}{dt}\bigg|_{\mathrm{ps}} \right\rangle_t = \beta\mu M K^{\mathrm{ps}}, \qquad (25)$$

which is a more generalized relationship at the NEPS to connect the time average of internal entropy production rate, the rate of work done to the system, and the net particle flow. Note that the relationship also holds for NESS in which these three variables are already time independent:

$$\frac{d_iS}{dt}\bigg|_{\mathrm{ss}} = -\beta \frac{dW}{dt}\bigg|_{\mathrm{ss}} = \beta\mu M K^{\mathrm{ss}}. \qquad (26)$$

IV. THREE-URN RING MODEL ($M = 3$)

In this section, we discuss the three-urn case because $M = 3$ is the minimal urn number to illustrate the NEPS, one of the NEAS never discussed before (only equilibrium states and NESSs in previous studies [33,34]). And since the phase space is two-dimensional, NEQPSs or NECSs are not possible in this case.

A. Phase diagram, NEPS, uniform, and nonuniform NESSs in the three-urn model

The phase diagram of the three-urn case is obtained from solving Eq. (5), which is shown in Fig. 2(a). At large g, the system is at a uNESS. When the particle interaction becomes more and more attractive, until $g < -3$, the uNESS becomes unstable. (In general, for arbitrary M, the uNESS is unstable when $g < -M$. See Appendix C for details.) The system is at a nuNESS at small unbalanced jumping rate, $p \gtrsim \frac{1}{2}$. By increasing p up to a critical value, the nuNESS becomes dynamically unstable via saddle-node bifurcation, i.e., Eq. (5) has no stable fixed point and the phase boundary (blue solid curve) has been determined analytically [34].

For $-3.8 \lesssim g < -3$ and large enough p, the NESS (uNESS or nuNESS) is unstable to the NEPS. It can be identified by observing $\xi_i(t)$ and $K_{i \to i+1}(t)$ in time asymptotically. Furthermore, by carefully examining the NEPS, it is found
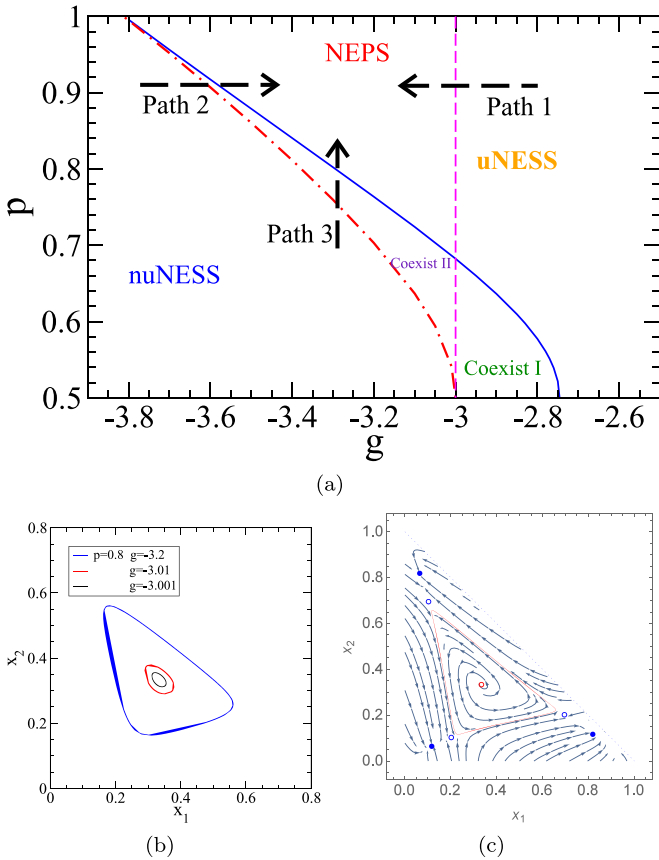
(a)

(b)

(c)

FIG. 2. (a) Phase diagram of three urn ring model. There are five regions, uniform nonequilibrium steady state (uNESS), nonuniform nonequilibrium steady state (nuNESS), coexistence of both uNESS and nuNESS (coexist I), nonequilibrium periodic state (NEPS), and coexistence of both NEPS and nuNESS (coexist II). Three routes to NEPS, path 1 (decreasing g at $p = 0.9$ from uNESS), path 2 (increasing g at $p = 0.9$ from nuNESS), and path 3 (increasing p at $g = -3.3$ from nuNESS). (b) The long-time trajectories in the NEPS for $p = 0.8$ and $g = -3.2$, 3.01. Very close to the Hopf bifurcation point, the oscillation just emerges with very small amplitude ($g = -3.001$) is also shown. (c) The phase portrait in the coexist II regime with $p = 0.8$ and $g = -3.35$. The periodic trajectory (red closed curve) coexists with the stable fixed points of the nuNESSs (filled blue circles), the corresponding unstable fixed points are also shown by the open blue circles. The unstable uNESS fixed point is marked by an open red circle.

that there is a coexistence regime (coexist II region bounded by the solid blue curve and red dot-dashed curve in Fig. 2(a)] in which the nuNESS coexists with the NEPS. The phase boundary (red dot-dashed curve) at which the NEPS vanishes via an infinite-period global bifurcation is obtained from the numerical solution of Eq. (5).

The nonequilibrium phase transition between the uNESS and NEPS (the dashed vertical line phase boundary) such as path 1 in Fig. 2(a) is characterized by a Hopf bifurcation in the dynamical system from Eq. (5). As g decreases along path 1, the uNESS becomes unstable and gives ways to stable periodic dynamics at $g = -3^-$ with finite period and infinitesimally small emerging oscillation amplitude as shown in the phase space trajectories in Fig. 2(b),
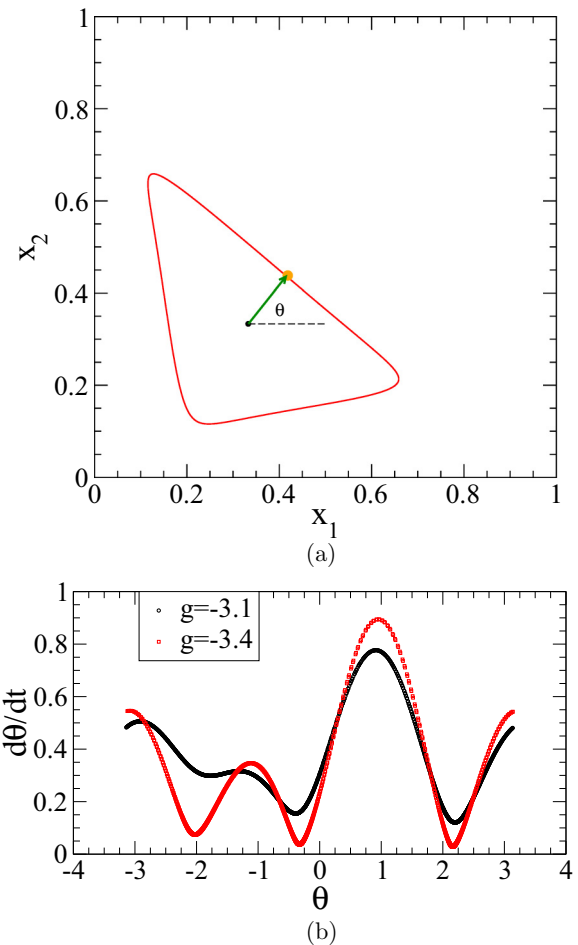

(a)

(b)

FIG. 3. (a) Periodic trajectory for the NEPS in the phase space with $p = 0.9$ and $g = -3.4$ undergoing a counter-clockwise circulation. The instantaneous of $\vec{\xi}(t)$ is marked by the filled orange dot whose location relative to $(\frac{1}{3}, \frac{1}{3})$ and can be represented by the angular variable $\theta(t)$ as shown. (b) $\dot{\theta}$ vs θ in the NEPS for $p = 0.9$ and $g = -3.1$ and -3.4.

characterized by a supercritical Hopf bifurcation. On the other hand, the nonequilibrium phase transition between the nuNESS and NEPS [the dot-dashed phase boundary in Fig. 2(a)] is characterized by an infinite-period global bifurcation. As demonstrated by the reverse path 3 in Fig. 2(a), the system is in a coexist II region in which the NEPS and NESS coexist before arriving at the phase boundary. As shown in the phase portrait Fig. 2(c), the periodic NEPS trajectory (red closed curve) coexists with three pairs of stable (filled blue circles) and unstable (open blue circles) fixed points of the nuNESSs. Further decrease in g will shift the periodic trajectory to be closer to the attracting manifold of the stable fixed point and hence increasing the oscillation period. Eventually, when g hits the phase boundary [red dot-dashed curve in Fig. 2(a)] and the trajectory falls onto the attractive fixed point and hence destroys the limit cycle, resulting in an infinite period global bifurcation. One can focus on the phase (angular) dynamics of the periodic dynamics of the NEPS, which can be characterized by the angular variable $\theta(t)$ as depicted in Fig. 3(a). The effective phase dynamics
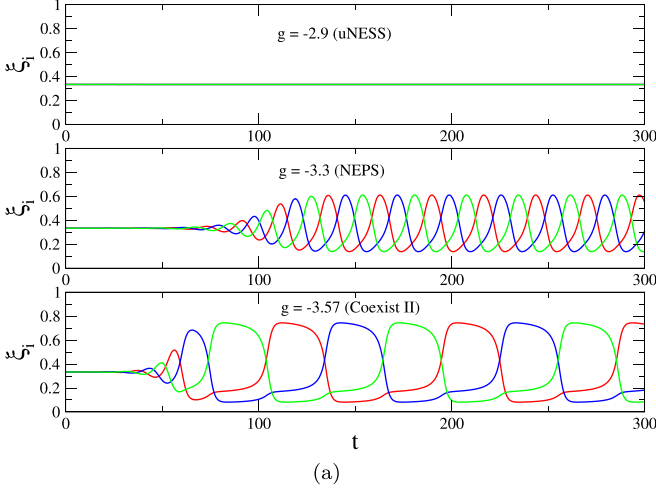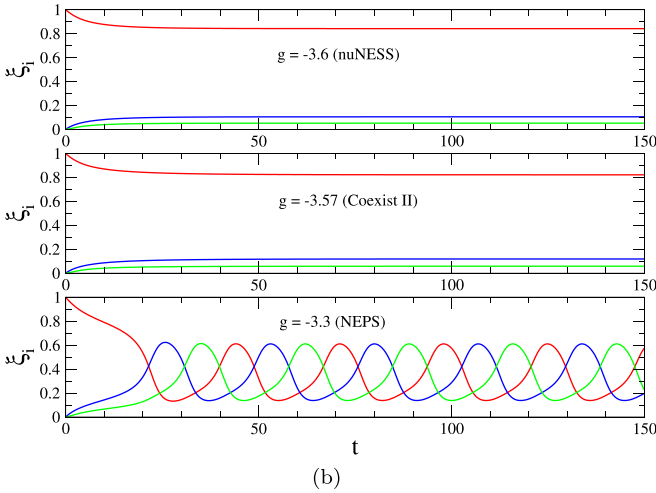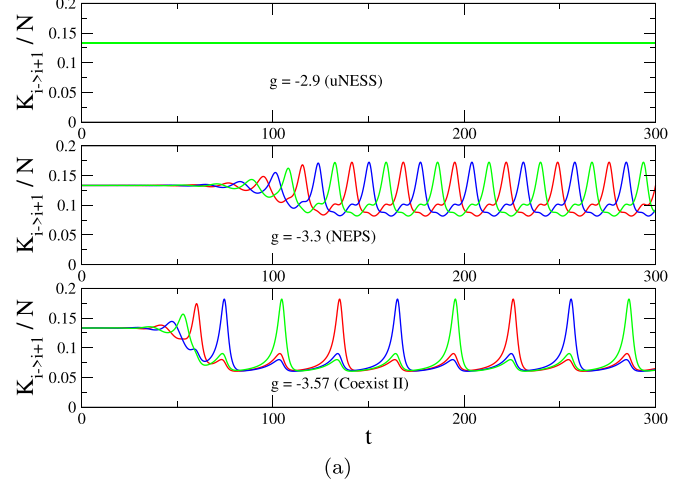
FIG. 4. $\xi_i(t)$ are plotted as a function of t at different g with $p = 0.9$. ξ_1, ξ_2, and $\xi_3 = 1 - \xi_1 - \xi_2$ are represented by red, blue, and green lines, respectively. The result is numerically solved from Eq. (5). (a) The graphs correspond to path 1 in Fig. 2(a) with initial condition $\vec{\xi}(0) = (\frac{1}{3}, \frac{1}{3}, \frac{1}{3})$. (b) The graphs correspond to path 2 in Fig. 2(a) with initial condition $\vec{\xi}(0) = (1, 0, 0)$.

FIG. 5. $K_{i \rightarrow i+1}(t)/N$ are plotted as a function of t at different g with $p = 0.9$. $K_{1 \rightarrow 2}$, $K_{2 \rightarrow 3}$, and $K_{3 \rightarrow 1}(=K_{0 \rightarrow 1})$ are represented by red, blue, and green lines, respectively. The result is numerically solved from Eq. (20). (a) The graphs correspond to path 1 in Fig. 2(a) with initial condition $\vec{\xi}(0) = (\frac{1}{3}, \frac{1}{3}, \frac{1}{3})$. (b) The graphs correspond to path 2 in Fig. 2(a) with initial condition $\vec{\xi}(0) = (1, 0, 0)$.
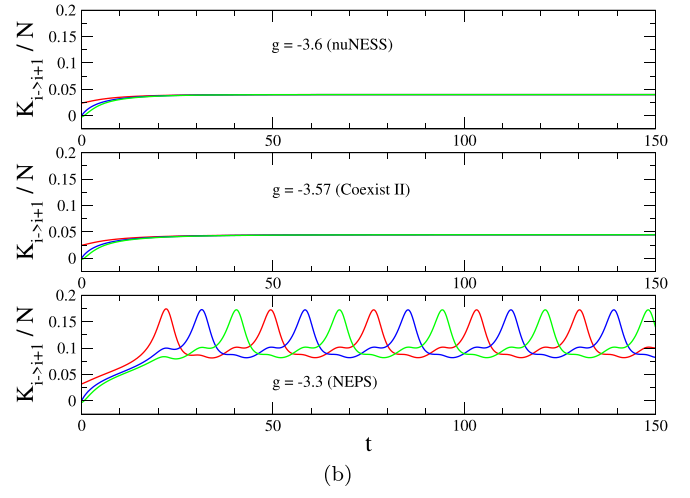
can be obtained by plotting $\dot{\theta}$ vs θ as shown in Fig. 3(b). As the system approaches the phase boundary [dot-dashed curve in Fig. 2(a)], the minima of $\dot{\theta}$ approach zero, signifying the infinite period global bifurcation for the vanishing of the NEPS. The period of the NEPS has a one-over-square-root divergence following the classic scenario of critical slowing down in infinite period bifurcation [39].

B. Nonequilibrium fluxes and periodic oscillations

To further examine the NEPS, three routes from NESS to NEPS, which are paths 1, 2, 3 shown in Fig. 2(a), are studied. Figures 4 and 5 show $\xi_i(t)$ and $K_{i \rightarrow i+1}(t)$ at different g with fixed $p = 0.9$, respectively. The right and left columns correspond to paths 1 and 2, respectively. It is seen that $\xi_i(t)$ and $K_{i \rightarrow i+1}(t)$ become periodic asymptotically at the NEPS. In addition, the coexistence of nuNESS and NEPS (coexist II regime) is explicitly demonstrated that for $g = -3.57$,

nuNESS results in path 2 but path 1 leads to NEPS due to different different initial conditions.

Figures 6 and 7 show $\xi_i(t)$ and $K_{i \rightarrow i+1}(t)$ at different p with fixed $g = -3.3$, respectively. It corresponds to path 3. $\xi_i(t)$ and $K_{i \rightarrow i+1}(t)$ become periodic asymptotically, arriving at the NEPS for large p. Between nuNESS and NEPS, there is a coexistence region labeled by coexist II. The asymptotic behavior of $\xi_i(t)$ and $K_{i \rightarrow i+1}(t)$ will depend on the initial condition. It can be a nuNESS or NEPS asymptotically, as illustrated in the $p = 0.78$ panels in Figs. 6 and 7.

As shown in Fig. 8, when the system from NEPS approaches the phase boundary of uNESS by increasing g at fixed $p = 0.9$ (reversed path 1), the amplitude of occupation oscillation, $\max(\xi_i^{\text{ps}}(t)) - \frac{1}{3}$, drops to zero continuously whereas the corresponding oscillation period (T) decreases to a finite value. Such a behavior indicates clearly that the transition between uNESS and NEPS at $g = -3$ is via a supercritical Hopf bifurcation. Furthermore, for $g \rightarrow -3^-$,
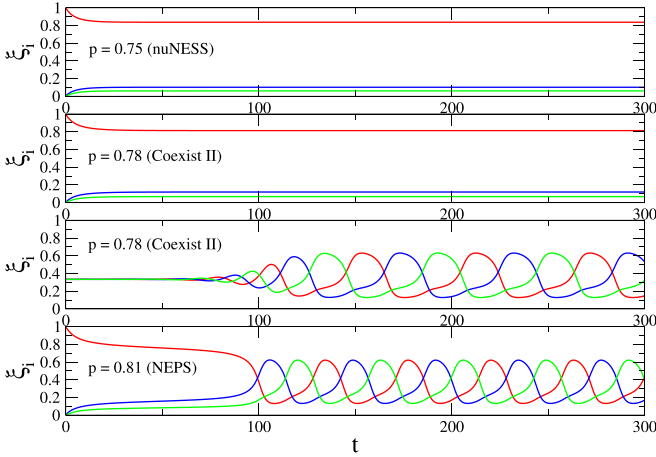
FIG. 6. $\xi_i(t)$ are plotted as a function of t at $p = 0.75, 0.78, 0.81$ with $g = -3.3$. ξ_1, ξ_2, and $\xi_3 = 1 - \xi_1 - \xi_2$ are represented by red, blue, and green lines, respectively. The initial conditions are $\vec{\xi}(0) = (1, 0, 0)$, except that it is $\vec{\xi}(0) = (\frac{1}{3}, \frac{1}{3}, \frac{1}{3})$ in the third row. The result is numerically solved from Eq. (5). The graphs correspond to path 3 in Fig. 2(a).

$|\xi_i^{\mathrm{ps}}(t) - \frac{1}{3}| \ll 1$, Eq. (5) can be linearized as

$$\frac{d}{dt}\begin{pmatrix} \xi_1^{\mathrm{ps}}(t) - \frac{1}{3} \\ \xi_2^{\mathrm{ps}}(t) - \frac{1}{3} \end{pmatrix} = -\frac{1}{4}(p - q)\begin{pmatrix} 1 & 2 \\ -2 & -1 \end{pmatrix}\begin{pmatrix} \xi_1^{\mathrm{ps}}(t) - \frac{1}{3} \\ \xi_2^{\mathrm{ps}}(t) - \frac{1}{3} \end{pmatrix},$$

(27)

which gives

$$\frac{2\pi}{T} = \frac{\sqrt{3}}{4}(p - q) \quad \text{or} \quad T = \frac{8\pi}{\sqrt{3}(p - q)}. \quad (28)$$

The above formula is in agreement with the numerical value near phase boundary with $g \lesssim -3$, as shown in Fig. 9(b).
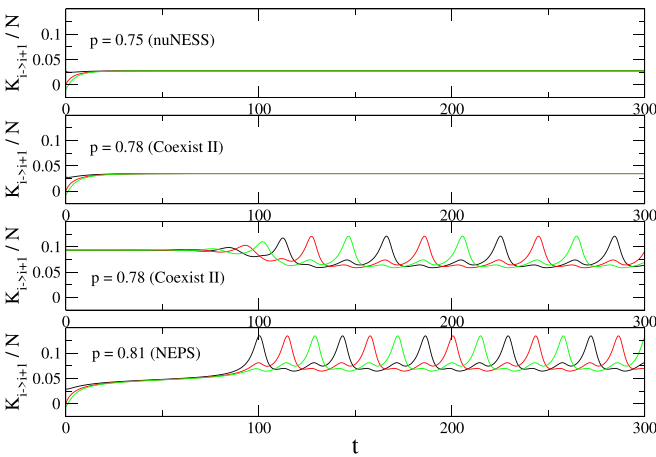

FIG. 7. $K_{i \to i+1}(t)/N$ are plotted as a function of t at $p = 0.75, 0.78, 0.81$ with $g = -3.3$. $K_{1 \to 2}$, $K_{2 \to 3}$, and $K_{3 \to 1}(= K_{0 \to 1})$ are represented by red, blue, and green lines, respectively. The initial conditions are $\vec{\xi}(0) = (1, 0, 0)$, except that it is $\vec{\xi}(0) = (\frac{1}{3}, \frac{1}{3}, \frac{1}{3})$ in the third row. The result is numerically solved from Eq. (20). The graphs correspond to the path 3 in Fig. 2(a).
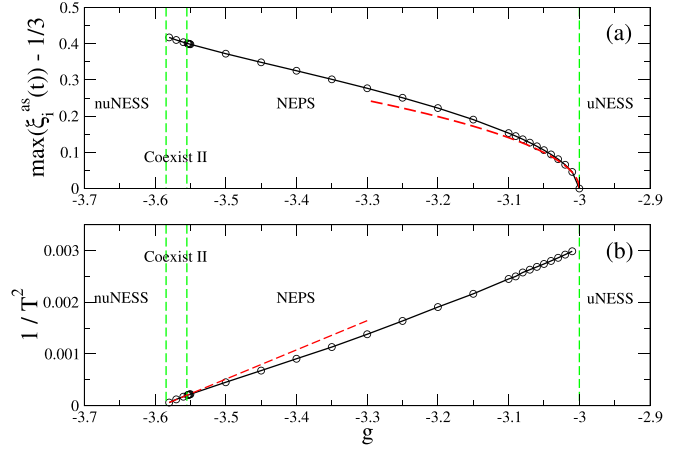

FIG. 8. (a) The amplitude of occupation oscillation, $\max(\xi_i^{\mathrm{ps}}(t)) - \frac{1}{3}$, is plotted as a function of g at $p = 0.9$ at NEPS. Red dashed line is the analytical result near phase boundary from Eq. (36). (b) The inverse of square of oscillation period, $1/T^2$, is plotted as a function of g at $p = 0.9$ at NEPS. Red dashed line is the linear fitting near phase boundary. The vertical dashed lines are the phase boundaries.

To capture the behavior of the amplitude of occupation oscillation, define $\eta_i^{\mathrm{ps}}(t) \equiv \xi_i^{\mathrm{ps}}(t) - \frac{1}{3}$. Considering only the first harmonic component in Eq. (14), one gets

$$\eta_1^{\mathrm{ps}}(t) = \eta^{\mathrm{ps}} \cos\left(\frac{2\pi}{T}t\right), \quad (29)$$

$$\eta_2^{\mathrm{ps}}(t) = \eta^{\mathrm{ps}} \cos\left(\frac{2\pi}{T}t - \frac{2\pi}{3}\right), \quad (30)$$

where η^{ps} is an undetermined time-independent coefficient corresponding to c_1 in Eq. (14). From Eqs. (29) and (30), one can show that

$$(\eta^{\mathrm{ps}})^2 = \frac{4}{3}\left[\left(\eta_1^{\mathrm{ps}}(t)\right)^2 + \left(\eta_2^{\mathrm{ps}}(t)\right)^2 + \eta_1^{\mathrm{ps}}(t)\eta_2^{\mathrm{ps}}(t)\right]. \quad (31)$$
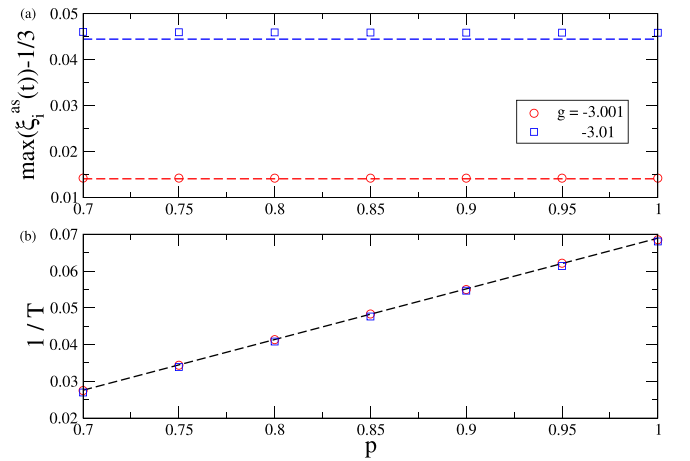

FIG. 9. (a) The amplitude of occupation oscillation, $\max(\xi_i^{\mathrm{ps}}(t)) - \frac{1}{3}$, is plotted as a function of p at $g = -3.001, -3.01$ at NEPS. Dashed lines are the corresponding analytical result from Eq. (36). (b) The inverse of oscillation period, $1/T$, is plotted as a function of p at $g = -3.001, -3.01$ at NEPS. The dashed line is the analytical result from Eq. (28).

Suppose the system is now near the phase boundary from NEPS to uNESS, i.e., $g \to -3^-$, and the current $\tilde{\eta}(t)$ is approaching η^{ps} in time. Then

$$\frac{d}{dt}(\tilde{\eta}(t))^2 \simeq \frac{4}{3}\frac{d}{dt}[(\tilde{\eta}_1(t))^2 + (\tilde{\eta}_2(t))^2 + \tilde{\eta}_1(t)\tilde{\eta}_2(t)]$$
$$= \frac{4}{3}\left[(2\tilde{\eta}_1 + \tilde{\eta}_2)\frac{d\tilde{\eta}_1}{dt} + (\tilde{\eta}_1 + 2\tilde{\eta}_2)\frac{d\tilde{\eta}_2}{dt}\right]. \quad (32)$$

Near the phase boundary, $\tilde{\eta}_i$ is small. Expand $A_i(\frac{1}{3} + \tilde{\eta}_1, \frac{1}{3} + \tilde{\eta}_2)$ from Eq. (9) up to $O((\tilde{\eta}_i)^3)$, which gives

$$\frac{d\tilde{\eta}_1}{dt} = -\frac{1}{4}(g + 2p + 2)\tilde{\eta}_1 - \left(p - \frac{1}{2}\right)\tilde{\eta}_2 + \frac{g}{4}(3p - 2)(\tilde{\eta}_1)^2$$
$$+ \frac{g}{2}(3p - 1)\tilde{\eta}_1\tilde{\eta}_2 + \frac{g}{4}(\tilde{\eta}_2)^2$$
$$+ \frac{g^3}{16}(\tilde{\eta}_1)^3 + \frac{g^3}{16}(\tilde{\eta}_1)^2\tilde{\eta}_2 + \frac{g^3}{16}\tilde{\eta}_1(\tilde{\eta}_2)^2, \quad (33)$$

$$\frac{d\tilde{\eta}_2}{dt} = -\left(q - \frac{1}{2}\right)\tilde{\eta}_1 - \frac{1}{4}(g + 2q + 2)\tilde{\eta}_2 + \frac{g}{4}(\tilde{\eta}_1)^2$$
$$+ \frac{g}{2}(3q - 1)\tilde{\eta}_1\tilde{\eta}_2 + \frac{g}{4}(3q - 2)(\tilde{\eta}_2)^2$$
$$+ \frac{g^3}{16}(\tilde{\eta}_1)^2\tilde{\eta}_2 + \frac{g^3}{16}\tilde{\eta}_1(\tilde{\eta}_2)^2 + \frac{g^3}{16}(\tilde{\eta}_2)^3. \quad (34)$$

Substitute Eqs. (33) and (34) into Eq. (32), and since $\tilde{\eta}(t)$ is slowly varying compared with the oscillation of period T, the quasistatic approximation [40] is applied such that $\tilde{\eta}_1^m(t)\tilde{\eta}_2^n(t) \simeq \tilde{\eta}^{m+n}(t)\langle\cos^m(\frac{2\pi}{T}t)\cos^n(\frac{2\pi}{T}t - \frac{2\pi}{3})\rangle_t$. After some algebra, we have

$$\frac{d}{dt}\tilde{\eta}^2 = \frac{1}{2}(g + 3)\tilde{\eta}^2 + \frac{3}{32}(-g)^3\tilde{\eta}^4. \quad (35)$$

When $g \lesssim -3$, $\frac{d}{dt}\tilde{\eta}^2 = 0$ gives only one stable fixed point $\tilde{\eta}^2 = -\frac{16}{3(-g)^3}(g + 3)$, which gives the oscillation amplitude:

$$\eta^{ps} = \frac{4}{|g|}\left|\frac{g+3}{3g}\right|^{\frac{1}{2}} \simeq \frac{4}{9}|g + 3|^{\frac{1}{2}}. \quad (36)$$

This analytical result is consistent with the numerical values near the phase boundary, $g \lesssim -3$, as shown by the dashed fitted curve in Fig. 8(a) and also in Fig. 9(a). Since η^{ps} drops to zero continuously from NEPS to uNESS, $\xi^{ps}(t)$ approaches ξ^{ss} and $K_{i \to i+1}^{ps}(t)$ will also approach K^{ss}.

On the other hand, when the system transits from NEPS to nuNESS, there appears a coexistence region in between the two phase boundaries as shown in Fig. 2(a). In particular, the vanishing of the NEPS is via an infinite-period global bifurcation at which the period of oscillation diverges, but the oscillation amplitude remains finite [see Fig. 8(a)] as the phase boundary is approached, as discussed in the previous section. Such behavior is confirmed in the plot of $1/T^2$ vs g in Fig. 9(b) for fixed $p = 0.9$ [path 2 in Fig. 2(a)], showing a linear behavior (dashed straight line) near the phase boundary. Figure 10 demonstrates a similar behavior characterized by the infinite-period global bifurcation as p is varied with fixed $g = -3.3$ [path 3 in Fig. 2(a)].
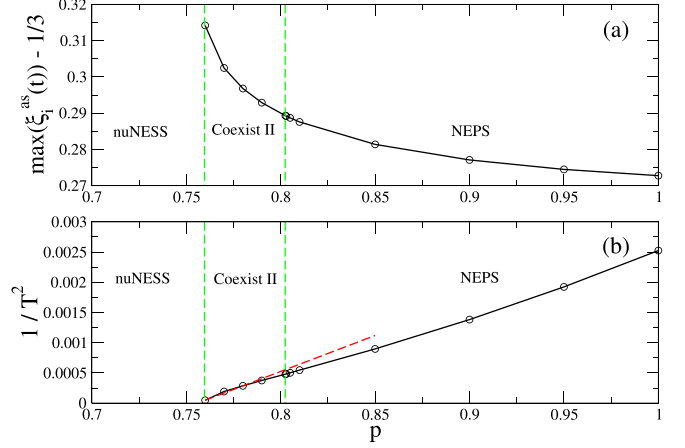

FIG. 10. (a) The amplitude of occupation oscillation, $\max(\xi_i^{ps}(t)) - \frac{1}{3}$, is plotted as a function of p at $g = -3.3$ at NEPS. (b) The inverse of square of oscillation period, $1/T^2$, is plotted as a function of p at $g = -3.3$ at NEPS. Red dashed line is the linear fitting near the phase boundary verifying the infinite-period bifurcation characteristics. The vertical dashed lines are the phase boundaries.

C. Nonuniformity and entropy production

The mean particle flux in the NEAS can be measured by the time average of the flux by $K^{as} \equiv \langle K_{1 \to 2}^{as}(t)\rangle_t = \langle K_{2 \to 3}^{as}(t)\rangle_t = \langle K_{3 \to 1}^{as}(t)\rangle_t$. The mean nonuniformity in the NEAS can also be defined in a similar way from Eq. (12). Figures 11 and 12 show K^{as}/N and $\psi^{as} \equiv \langle\psi^{as}(t)\rangle_t$ at different g with fixed $p = 0.9$ and at different p with fixed $g = -3.3$, which cover NESS, NEPS, and their coexistence. The mean flux, in general, increases with p (the driving of the system) and decreases with the interparticle attraction ($|g|$). The mean nonuniformity, in general, decreases with p but increases with the interparticle attraction ($|g|$).

When the system is out of equilibrium, the entropy production does not vanish. The time average $\langle\frac{dS}{dt}\rangle_t = \langle\frac{dE}{dt}\rangle_t = 0$ for equilibrium state, NESS, and NEPS. According to the thermodynamic law in Eq. (13) and also from Eq. (23), we
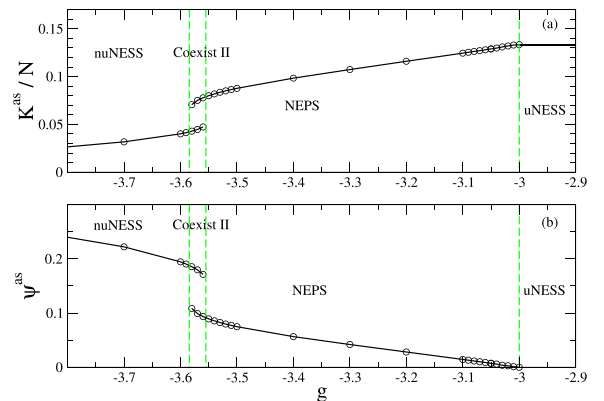

FIG. 11. (a) K^{as}/N are plotted as a function of g at $p = 0.9$. (b) $\psi^{as} \equiv \langle\psi^{as}(t)\rangle_t$ are plotted as a function of g at $p = 0.9$. For $g > -3$ at uNESS, $\psi^{as} \equiv \psi^{ss} = 0$. The vertical dashed lines are the phase boundaries.

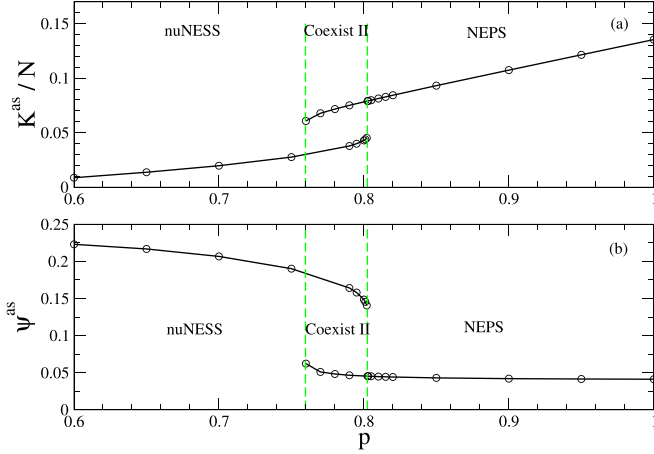FIG. 12. (a) K^{as}/N are plotted as a function of p at $g = -3.3$. $K^{as} \equiv \langle K^{as}_{1 \to 2}(t) \rangle_t = \langle K^{as}_{2 \to 3}(t) \rangle_t = \langle K^{as}_{3 \to 1}(t) \rangle_t$ and (b) $\psi^{as} \equiv \langle \psi^{as}(t) \rangle_t$ are plotted as a function of p at $g = -3.3$. The vertical dashed lines are the phase boundaries.

arrive at

$$\left\langle \frac{d_i S}{dt} \right\rangle_t = 3K^{as} \ln\left(\frac{p}{q}\right) \qquad (37)$$

by noticing $\mu = \beta^{-1} \ln(\frac{p}{q})$ and $K^{as} \equiv \langle K^{as}_{1 \to 2}(t) \rangle_t = \langle K^{as}_{2 \to 3}(t) \rangle_t = \langle K^{as}_{3 \to 1}(t) \rangle_t$. Here the superscript stands for equilibrium state, NESS, or NEPS.

Since both the entropy production and nonuniformity depend on the degree of nonequilibrium or orderliness of the system, one may suspect they are related. As shown in Fig. 13, when the relationship between ψ^{as} and $\frac{K^{as}}{N(p-q)}$ for different p at different kinds of NEAS are plotted, all data collapsed into a single universal curve. It suggests a general relation

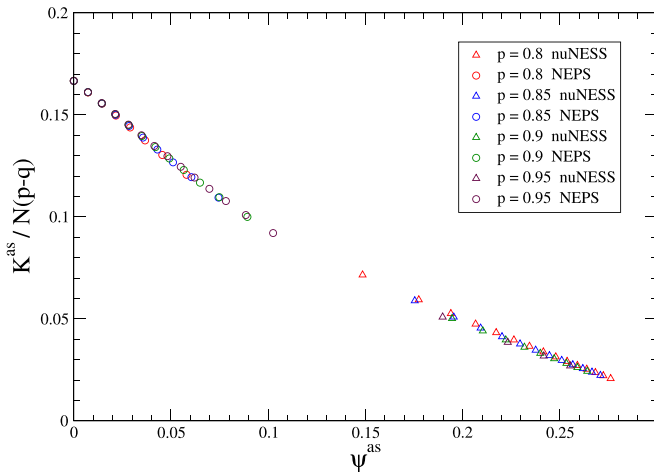$$\left\langle \frac{d_i S}{dt} \right\rangle_t = N\Phi(\psi^{as})(p-q)\ln\left(\frac{p}{q}\right), \qquad (38)$$

FIG. 13. The relationship between $\psi^{as} \equiv \langle \psi^{as}(t) \rangle_t$ and $\frac{K^{as}}{N(p-q)}$ for different p at different kinds of NEAS. The data points fall onto a single curve.

where the function $\Phi(\psi^{as})$ is some decreasing function, i.e., $\Phi'(\psi^{as}) < 0$. It is a generalization of the same entropy-production-nonuniformity relation from NESS [34] to NEPS.

Furthermore, by rewriting Eq. (38) as

$$\left\langle \frac{d_i S}{dt} \right\rangle_t = h\left(\left|p - \frac{1}{2}\right|\right)/(1/\Phi),$$

$$h(x) \equiv 2Nx \ln\left(\frac{\frac{1}{2}+x}{\frac{1}{2}-x}\right), \qquad (39)$$

it contains the flavor of a generalized fluctuation-dissipation relation for NEAS when compared to the usual fluctuation-dissipation relation relating the damping coefficient and diffusion constant at equilibrium: $\gamma = \frac{k_B T}{D}$. Here the mean entropy production is the dissipation and $1/\Phi$ increases with the nonuniformity and hence is a measure of the fluctuation of the NEAS. The driving source for maintaining the NEAS here is $h(|p - \frac{1}{2}|)$, instead of the thermal energy $k_B T$ for the equilibrium case.

V. FLUCTUATION EFFECTS

In the previous sections, only the optimal point solutions were discussed. However, near the phase boundary, the fluctuation effect may be significant (cf. during continuous phase transition at equilibrium).

Let $\vec{y} \equiv \vec{x} - \vec{\xi}(t)$. From Eq. (3), $\rho(\vec{y}, t) \propto \exp[N \sum_{i,j=1}^{M-1} c_{ij}(t) y_i y_j]$. Notice that $\sum_{i=1}^{M} y_i = 0$, $\langle y_i \rangle = 0$, and from Eq. (12), one can decompose the nonuniformity into the mean and fluctuating parts:

$$\psi(t) = \frac{1}{M(M-1)} \sum_{(i<j)=1}^{M} (\xi_i(t) - \xi_j(t))^2$$

$$+ \frac{2}{M-1} \sum_{(i \leqslant j)=1}^{M-1} \langle y_i y_j \rangle$$

$$= \frac{1}{M(M-1)} \sum_{(i<j)=1}^{M} (\xi_i(t) - \xi_j(t))^2$$

$$+ \frac{1}{N} \frac{2}{M-1} \sum_{(i \leqslant j)=1}^{M-1} (\mathbf{c}^{-1})_{ij}(t)$$

$$\equiv \psi^{(0)}(t) + \frac{1}{N}\psi^{(1)}(t), \qquad (40)$$

where $\psi^{(0)}$ is the thermodynamic limit and $\psi^{(1)}$ is the fluctuation. Take three urns, $M = 3$, as an example. When the system approaches the phase boundary from uNESS, $\vec{\xi}^{ss} = (\frac{1}{3}, \frac{1}{3}, \frac{1}{3})$, $\psi^{ss(0)} = 0$, $\psi^{ss(1)} = -\frac{2}{g+3}$, which diverges at $g \to -3^+$. However, the nonuniformity itself in thermodynamic limit still converges to zero, $\lim_{g \to -3^+} \lim_{N \to \infty} \psi(t) = 0$, showing that the fluctuation effect doesn't take place in nonuniformity.

To capture the fluctuation effect in observation, we consider the net particle flow fluctuation $\frac{1}{N} \langle (\delta K_{i \to i+1}(\vec{x}))^2 \rangle$. Note the continuous form of Eq. (20) is

$$K_{i \to i+1}(t) = N \int d^{M-1} y \rho(\vec{y}, t) \tilde{K}_{i \to i+1}(\vec{y}, t), \qquad (41)$$

where

$$
\begin{aligned}
&\tilde{K}_{i \to i+1}(\vec{y}, t) \\
&= \frac{p(y_i + \xi_i)e^{g(y_i+\xi_i)} - q(y_{i+1} + \xi_{i+1})e^{g(y_{i+1}+\xi_{i+1})}}{e^{g(y_i+\xi_i)} + e^{g(y_{i+1}+\xi_{i+1})}},
\end{aligned}
$$

then the net flow fluctuation

$$
\begin{aligned}
&\frac{1}{N}\langle (\delta K_{i \to i+1}(\vec{x}))^2 \rangle \\
&= \frac{1}{N}\left(\langle K_{i \to i+1}^2(\vec{x}) \rangle - \langle K_{i \to i+1}(\vec{x}) \rangle^2 \right) \\
&= N\left((\partial_i \tilde{K}_{i \to i+1}(0))^2 \langle y_i^2 \rangle + (\partial_{i+1} \tilde{K}_{i \to i+1}(0))^2 \langle y_{i+1}^2 \rangle \right. \\
&\quad \left. + 2(\partial_i \tilde{K}_{i \to i+1}(0))(\partial_{i+1} \tilde{K}_{i \to i+1}(0))\langle y_i y_{i+1} \rangle + O\left(\frac{1}{N}\right) \right) \\
&= -(\partial_i \tilde{K}_{i \to i+1}(0))^2 (\mathbf{c}^{-1})_{ii} - (\partial_{i+1} \tilde{K}_{i \to i+1}(0))^2 (\mathbf{c}^{-1})_{i+1,i+1} \\
&\quad - 2(\partial_i \tilde{K}_{i \to i+1}(0))(\partial_{i+1} \tilde{K}_{i \to i+1}(0))(\mathbf{c}^{-1})_{i,i+1} + O\left(\frac{1}{N}\right),
\end{aligned}
\tag{42}
$$

where

$$
\begin{aligned}
\partial_i \tilde{K}_{i \to i+1}(0) &= \frac{p}{e^{-g(\xi_i - \xi_{i+1})} + 1} \\
&\quad + \frac{pg\xi_i}{(e^{-g(\xi_i-\xi_{i+1})} + 1)(e^{-g(\xi_{i+1}-\xi_i)} + 1)}
\end{aligned}
$$

$$
\begin{aligned}
\partial_{i+1} \tilde{K}_{i \to i+1}(0) &= -\frac{q}{e^{-g(\xi_{i+1}-\xi_i)} + 1} \\
&\quad - \frac{qg\xi_{i+1}}{(e^{-g(\xi_i-\xi_{i+1})} + 1)(e^{-g(\xi_{i+1}-\xi_i)} + 1)}.
\end{aligned}
$$

In particular, for $M = 3$, when the system approaches the phase boundary from uNESS, $g > -3$, from Appendix B, one has

$$
(\mathbf{c}^{ss})^{-1} = -\frac{2}{3(g+3)}\begin{pmatrix} 2 & -1 \\ -1 & 2 \end{pmatrix},
\tag{43}
$$

and hence

$$
\frac{1}{N}\langle (\delta K_{i \to i+1}^{ss}(\vec{x}))^2 \rangle = \frac{(1-pq)}{24}\frac{1}{g+3} + O\left(\frac{1}{N}\right),
\tag{44}
$$

which is divergent as $g \to -3^+$.

To get the net flow fluctuation at NEPS, one has to first solve for $(\mathbf{c}^{ps})^{-1}$ from Eq. (6). Near the phase boundary from NEPS, at $g \to -3^-$, $|\xi_i^{ps}(t) - \frac{1}{3}| = |\eta_i^{ps}(t)| \ll 1$. Expanding $A_i(\xi_1^{ps}(t), \xi_2^{ps}(t))$ around $(\frac{1}{3}, \frac{1}{3})$ up to $O((\eta^{ps})^3)$, and then applying the quasistatic approximation, one would get

$$
\begin{aligned}
\mathbf{a}^{ps} &\equiv \begin{pmatrix} \partial_1 A_1(\xi_1^{ps}(t), \xi_2^{ps}(t)) & \partial_2 A_1(\xi_1^{ps}(t), \xi_2^{ps}(t)) \\ \partial_1 A_2(\xi_1^{ps}(t), \xi_2^{ps}(t)) & \partial_2 A_2(\xi_1^{ps}(t), \xi_2^{ps}(t)) \end{pmatrix} \\
&\simeq \begin{pmatrix} -\frac{1}{4}(g + 2p + 2) + \frac{3}{32}g^3(\eta^{ps})^2 & -\frac{1}{2}(p - q) \\ \frac{1}{2}(p - q) & -\frac{1}{4}(g + 2q + 2) + \frac{3}{32}g^3(\eta^{ps})^2 \end{pmatrix} \\
&\simeq -\frac{1}{4}\begin{pmatrix} |g + 3| + (p - q) & 2(p - q) \\ -2(p - q) & |g + 3| - (p - q) \end{pmatrix},
\end{aligned}
\tag{45}
$$

and assume

$$
\begin{aligned}
\mathbf{b}^{ps} &\equiv \begin{pmatrix} B_{11}(\xi_1^{ps}(t), \xi_2^{ps}(t)) & B_{12}(\xi_1^{ps}(t), \xi_2^{ps}(t)) \\ B_{21}(\xi_1^{ps}(t), \xi_2^{ps}(t)) & B_{22}(\xi_1^{ps}(t), \xi_2^{ps}(t)) \end{pmatrix} \\
&\simeq \begin{pmatrix} B_{11}(\frac{1}{3}, \frac{1}{3}) & B_{12}(\frac{1}{3}, \frac{1}{3}) \\ B_{21}(\frac{1}{3}, \frac{1}{3}) & B_{22}(\frac{1}{3}, \frac{1}{3}) \end{pmatrix} \\
&= \frac{1}{6}\begin{pmatrix} 2 & -1 \\ -1 & 2 \end{pmatrix}.
\end{aligned}
\tag{46}
$$

By quasistatic approximation, $\frac{d}{dt}(\mathbf{c}^{ps})^{-1} = 0$, then Eq. (6) is reduced to $\mathbf{a}^{ps}(\mathbf{c}^{ps})^{-1} + (\mathbf{c}^{ps})^{-1}(\mathbf{a}^{ps})^t = 2\mathbf{b}^{ps}$, which gives

$$
(\mathbf{c}^{ps})^{-1} = -\frac{2}{3|g+3|}\begin{pmatrix} 2 & -1 \\ -1 & 2 \end{pmatrix}.
\tag{47}
$$

From Eq. (42), one gets

$$
\frac{1}{N}\langle\langle (\delta K_{i \to i+1}^{ps}(\vec{x}))^2 \rangle\rangle_t = \frac{(1-pq)}{24}\frac{1}{|g+3|} + O\left(\frac{1}{N}\right),
\tag{48}
$$

which is divergent as $g \to -3^-$.

In the previous section, at NEPS, one gets the oscillation amplitude of the occupation number, which is equivalent to η^{ps} expressed in Eq. (36). This amplitude is derived from the dynamical equation in Eq. (5). However, it is also interesting to study its thermal fluctuation effect, especially near the phase transition. Define the stochastic variable

$$
\eta^2(t) \equiv \frac{4}{3}\left[(x_1 - \tfrac{1}{3})^2 + (x_2 - \tfrac{1}{3})^2 + (x_1 - \tfrac{1}{3})(x_2 - \tfrac{1}{3})\right].
\tag{49}
$$

Notice that it is different from the deterministic variable $\tilde{\eta}(t)$ in Eq. (32). In the following, we are going to show that $\langle\langle \eta^2(t) \rangle\rangle_t = (\eta^{ps})^2$ in the thermodynamic limit.

Let $y_i \equiv x_i - \xi_i^{ps} = x_i - \frac{1}{3} - \eta_i^{ps}$, then

$$
\begin{aligned}
&\langle\langle \eta^2(t) \rangle\rangle_t \\
&= \frac{4}{3}\langle\langle (\eta_1^{ps} + y_1)^2 + (\eta_2^{ps} + y_2)^2 + (\eta_1^{ps} + y_1)(\eta_2^{ps} + y_2) \rangle\rangle_t
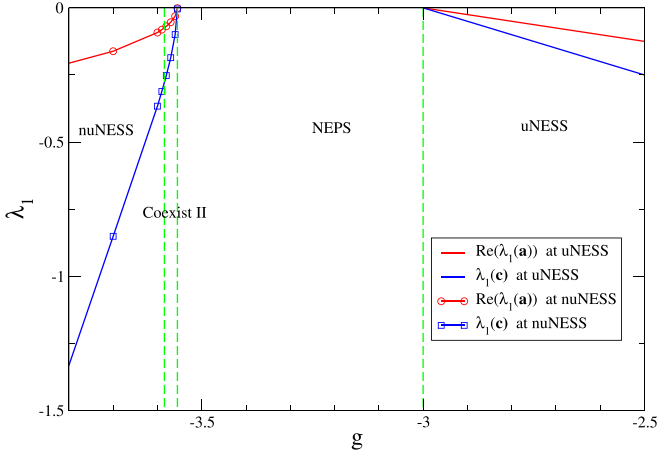\end{aligned}
$$

FIG. 14. The largest real parts of eigenvalues of $\mathbf{a}$, $\mathrm{Re}(\lambda_1(\mathbf{a}))$, and the largest eigenvalues of $\mathbf{c}$, $\lambda_1(\mathbf{c})$, are plotted as a function of g at $p = 0.9$. The vertical dashed lines are the phase boundaries. The graph corresponds to paths 1 and 2 in Fig. 2(a).

$$= \frac{4}{3}\langle (\eta_1^{\mathrm{ps}})^2 + (\eta_2^{\mathrm{ps}})^2 + \eta_1^{\mathrm{ps}}\eta_2^{\mathrm{ps}}\rangle_t + \frac{4}{3}\langle y_1^2 + y_2^2 + y_1 y_2\rangle$$
$$= (\eta^{\mathrm{ps}})^2 + O\left(\frac{1}{N}\right). \tag{50}$$

Its fluctuation is given by

$$N\langle\langle\delta\eta^2(t)\rangle\rangle_t \equiv N\left(\langle\langle\eta^4(t)\rangle\rangle_t - \langle\langle\eta^2(t)\rangle\rangle_t^2\right)$$
$$= \frac{8}{3}(\eta^{\mathrm{ps}})^2\langle y_1^2 + y_2^2 + y_1 y_2\rangle + O\left(\frac{1}{N^2}\right)$$
$$= \frac{128}{243} + O\left(\frac{1}{N^2}\right). \tag{51}$$

Thermal fluctuation would broaden the width of oscillation amplitude, but the width still keep a finite constant value near the phase boundary at $g \to -3^-$. For comparison, when the system approaches the phase boundary from uNESS, $g \to -3^+$, $N\langle\langle\delta\eta^2(t)\rangle\rangle_t = 0$.

Finally, the relation between the dynamical and thermodynamic instabilities are illustrated. At the NESS, the dynamical stability condition is that all real parts of eigenvalues of $\mathbf{a}$ are negative. Or, equivalently, the largest real parts of eigenvalues, $\mathrm{Re}(\lambda_1(\mathbf{a}))$, are negative. Similarly, the thermodynamic stability condition is that all eigenvalues of $\mathbf{c}$ are negative. Or, equivalently, the largest eigenvalues, $\lambda_1(\mathbf{c})$, are negative.

Figures 14 and 15 show $\mathrm{Re}(\lambda_1(\mathbf{a}))$ and $\lambda_1(\mathbf{c})$ at the NESS until it meets the phase boundaries. It is found that both $\mathrm{Re}(\lambda_1(\mathbf{a}))$ and $\lambda_1(\mathbf{c})$ approach zero from below. It implies the dynamical and thermodynamic instabilities occur simultaneously for both the uNESS and nuNESS. This result is consistent with the theorem presented in Appendix B. Thus, although we did not prove, in general, that thermodynamic stability implies dynamic stability, our example for the NESSs in the three-urn model supports the validity of the above assertion. In other words, the equivalence of dynamic and thermodynamic stability is demonstrated in the three-urn uNESS and nuNESS.
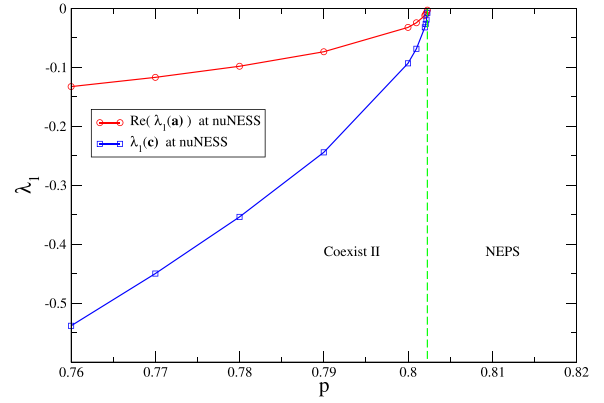

FIG. 15. The largest real parts of eigenvalues of $\mathbf{a}$, $\mathrm{Re}(\lambda_1(\mathbf{a}))$, and the largest eigenvalues of $\mathbf{c}$, $\lambda_1(\mathbf{c})$, are plotted as a function of p at $g = -3.3$. The vertical dashed line is the phase boundary. The graph corresponds to path 3 in Fig. 2(a).

VI. CONCLUSION

The NEAS is proposed and formulated in the framework of the Fokker-Planck equation under WKB approximation (thermodynamic limit). The NEAS is a generalization of the NESS, which also includes all other kinds of asymptotic states, such as the equilibrium state, NEPS, NEQPS, and NECS.

In our framework, the dynamics and thermodynamics of the system are not treated independently, but are mutually connected. It is shown that the dynamical stable NESS is always thermodynamically stable. The dynamical stability condition is that the real part of all eigenvalues of $\mathbf{a}$ are negative and thermodynamic stability condition is that all eigenvalues of $\mathbf{c}$ are negative. For a uNESS in the M urn-ring model, both dynamical and thermodynamic stability criteria are proved to be equivalent. For a nuNESS in the three-urn model, the above equivalence is also demonstrated. The NEPS is constructed in our framework and also illustrated in the Ehrenfest urn ring model and their time-average properties are calculated explicitly. Its physical properties such as the dissipation-nonuniformity relation and its transitions to NESS are illustrated.

Only the three-urn model is considered in this paper and the possible NEAS is limited to EQ, NESS, and NEPS. A larger number of urns on a ring will lead to a higher dimensional phase space, which allows the possibility of more complex dynamics such as NEQPS and NECS, which is under current study. Our theoretical framework can be extended to investigate the NECS that may enable one to distinguish chaotic and stochastic fluctuation in complex thermodynamic nonlinear systems.

APPENDIX A: ASYMPTOTIC STATE SOLUTION OF MULTIVARIATE LINEAR FOKKER-PLANCK EQUATION

The multivariate linear Fokker-Planck equation of dimension D for the asymptotic state reads

$$
\frac{\partial \rho^{\mathrm{as}}(\vec{x},t)}{\partial t}
$$

$$
= -\sum_{i=1}^{D} \frac{\partial}{\partial x_i}\left[\left(A_i(\vec{\xi}(t),t)+\sum_{j=1}^{D} a_{ij}(t)(x_j-\xi_j(t))\right)\rho^{\mathrm{as}}(\vec{x},t)\right]
$$

$$
+ \frac{1}{2N}\sum_{i,j=1}^{D} b_{ij}(t)\frac{\partial^2}{\partial x_i \partial x_j}\rho^{\mathrm{as}}(\vec{x},t), \tag{A1}
$$

where **a** and **b** are matrices of dimension $D \times D$. **b** is symmetric. In the large N limit, the form of the solution becomes

$$
\rho^{\mathrm{as}}(\vec{x},t) = \left(\frac{N}{\pi}\right)^{\frac{D}{2}} \det(-\mathbf{c})^{\frac{1}{2}} \exp
$$

$$
\times \left[N\sum_{i,j=1}^{D} c_{ij}(t)(x_i-\xi_i(t))(x_j-\xi_j(t))\right], \tag{A2}
$$

where **c** is a symmetric matrix determined by **a** and **b**. Substituting this form into Eq. (A1) and keeping the leading order in N, we get

$$
(\partial_t \vec{\xi})^{\mathrm{t}}\mathbf{c}\vec{y} = \vec{A}^{\mathrm{t}}\mathbf{c}\vec{y}, \tag{A3}
$$

$$
\vec{y}^{\mathrm{t}}(\partial_t \mathbf{c})\vec{y} = -2\vec{y}^{\mathrm{t}}\mathbf{c}\mathbf{a}\vec{y} + 2\vec{y}^{\mathrm{t}}\mathbf{c}\mathbf{b}\mathbf{c}\vec{y}, \tag{A4}
$$

where $\vec{y} \equiv \vec{x} - \vec{\xi}(t)$ for any $\vec{x}$. Equation (A3) is reduced to

$$
\partial_t \vec{\xi} = \vec{A}. \tag{A5}
$$

Note that **cbc** is symmetric but **ca** is not necessary to be. Using $\vec{y}^{\mathrm{t}}\mathbf{c}\mathbf{a}\vec{y} = \vec{y}^{\mathrm{t}}\mathbf{a}^{\mathrm{t}}\mathbf{c}\vec{y}$, Eq. (A4) can be rewritten as

$$
\vec{y}^{\mathrm{t}}(\partial_t \mathbf{c})\vec{y} = -\vec{y}^{\mathrm{t}}(\mathbf{c}\mathbf{a} + \mathbf{a}^{\mathrm{t}}c)\vec{y} + 2\vec{y}^{\mathrm{t}}\mathbf{c}\mathbf{b}\mathbf{c}\vec{y}, \tag{A6}
$$

which gives

$$
\partial_t \mathbf{c} = -\mathbf{c}\mathbf{a} - \mathbf{a}^{\mathrm{t}}c + 2\mathbf{c}\mathbf{b}\mathbf{c} \tag{A7}
$$

or, equivalently,

$$
\partial_t \mathbf{c}^{-1} = \mathbf{a}\mathbf{c}^{-1} + \mathbf{c}^{-1}\mathbf{a}^{\mathrm{t}} - 2\mathbf{b}, \tag{A8}
$$

which is a system of first-order differential equations of dimension $D(D+1)/2$ to uniquely determine the same number of independent matrix elements of **c**.

APPENDIX B: THEOREM FOR THE DYNAMICAL AND THERMODYNAMIC STABILITY OF NESS

Lemma (Lyapunov theorem [41]): Given the system of linear equation (the Lyapunov equation), $\mathbf{a}\mathbf{c}^{-1} + \mathbf{c}^{-1}\mathbf{a}^{\mathrm{t}} = 2\mathbf{b}$, where **b** is nonsingluar, symmetric, and positive definite, and all the real parts of eigenvalues of **a** are negative, $\mathrm{Re}(\lambda(\mathbf{a})) < 0$, then all the eigenvalues of **c** are real and negative, $\lambda(\mathbf{c}) < 0$.

Proof: Note that $\mathbf{c}^{-1}$ can be expressed as

$$
\mathbf{c}^{-1} = -2\int_0^\infty d\tau \mathrm{e}^{\tau\mathbf{a}}\mathbf{b}\mathrm{e}^{\tau\mathbf{a}^{\mathrm{t}}}, \tag{B1}
$$

which can checked by

$$
\mathbf{a}\mathbf{c}^{-1} + \mathbf{c}^{-1}\mathbf{a}^{\mathrm{t}} = -2\int_0^\infty d\tau(\mathbf{a}\mathrm{e}^{\tau\mathbf{a}}\mathbf{b}\mathrm{e}^{\tau\mathbf{a}^{\mathrm{t}}} + \mathrm{e}^{\tau\mathbf{a}}\mathbf{b}\mathrm{e}^{\tau\mathbf{a}^{\mathrm{t}}}\mathbf{a}^{\mathrm{t}})
$$

$$
= -2\int_0^\infty d\tau \frac{d}{d\tau}(\mathrm{e}^{\tau\mathbf{a}}\mathbf{b}\mathrm{e}^{\tau\mathbf{a}^{\mathrm{t}}})
$$

$$
= -2[\mathrm{e}^{\tau\mathbf{a}}\mathbf{b}\mathrm{e}^{\tau\mathbf{a}^{\mathrm{t}}}]_0^\infty
$$

$$
= 2\mathbf{b} \tag{B2}
$$

if the condition $\mathrm{Re}(\lambda(\mathbf{a})) < 0$ is imposed. Since **b** is nonsingular, then

$$
\mathbf{c} = -2\int_0^\infty d\tau \mathrm{e}^{-\tau\mathbf{a}^{\mathrm{t}}}\mathbf{b}^{-1}\mathrm{e}^{-\tau\mathbf{a}}. \tag{B3}
$$

Using the fact that **b** is symmetric and positive definite (so is $\mathbf{b}^{-1}$), we get that **c** is symmetric and negative definite, which implies all eigenvalues of **c** are real and negative. Q.E.D.

At the NESS, **a** and **c** defined in Eq. (4) are connected by the Lyapunov equation [Eq. (6) with $\partial_t \mathbf{c}^{-1} = 0$]. The dynamical stability condition is that the real part of all eigenvalues of **a** are negative and the thermodynamic stability condition is that all eigenvalues of **c** are negative. By the above lemma, we have the following theorem.

Theorem: At the NESS, the dynamical stability implies the thermodynamic stability.

In other words, thermodynamic instabililty at the NESS leads to dynamical instability.

APPENDIX C: STABILITY OF UNIFORM NONEQUILIBRIUM STEADY STATE

The Fokker-Planck Equation in Eq. (1) is reduced to Eq. (4) in the large N limit. For the uNESS in the M urn-ring model, when $M = 3$, from Eqs. (23) and (25) in Ref. [34], we have

$$
\mathbf{a} = -\frac{1}{2}\begin{pmatrix} 1+p+\frac{g}{2} & p-q \\ q-p & 1+q+\frac{g}{2} \end{pmatrix}, \tag{C1}
$$

in which its eigenvalues are $-\frac{g+3}{4} \pm i\frac{\sqrt{3}}{4}(p-q)$,

$$
\mathbf{c} = -\frac{g+3}{2}\begin{pmatrix} 2 & 1 \\ 1 & 2 \end{pmatrix}, \tag{C2}
$$

in which its eigenvalues are $-\frac{g+3}{2}$ and $-\frac{3(g+3)}{2}$. It can be seen that the real part of the eigenvalues of **a** and the eigenvalues of **c** are negative (positive) if $g > -3$ ($g < -3$). It implies the uNESS in the three-urn ring model is both dynamical and thermodynamically stable (unstable) if $g > -3$ ($g < -3$).

When $M \geqslant 4$,

$$
\mathbf{a} = -\frac{1}{2}
\begin{pmatrix}
1+p+\frac{3g}{2M} & p-q & p+\frac{g}{2M} & p+\frac{g}{2M} & \cdots & p+\frac{g}{2M} & p+\frac{g}{2M} & p+\frac{g}{2M} \\
-p-\frac{g}{2M} & 1+\frac{g}{M} & -q-\frac{g}{2M} & 0 & \cdots & 0 & 0 & 0 \\
0 & -p-\frac{g}{2M} & 1+\frac{g}{M} & -q-\frac{g}{2M} & \cdots & 0 & 0 & 0 \\
0 & 0 & -p-\frac{g}{2M} & 1+\frac{g}{M} & \cdots & 0 & 0 & 0 \\
\vdots & \vdots & \vdots & \vdots & \ddots & \vdots & \vdots & \vdots \\
0 & 0 & 0 & 0 & \cdots & 1+\frac{g}{M} & -q-\frac{g}{2M} & 0 \\
0 & 0 & 0 & 0 & \cdots & -p-\frac{g}{2M} & 1+\frac{g}{M} & -q-\frac{g}{2M} \\
q+\frac{g}{2M} & q+\frac{g}{2M} & q+\frac{g}{2M} & q+\frac{g}{2M} & \cdots & q+\frac{g}{2M} & q-p & 1+q+\frac{3g}{2M}
\end{pmatrix}
\tag{C3}
$$

and

$$
\mathbf{b} = \frac{1}{2M}
\begin{pmatrix}
2 & -1 & 0 & \cdots & 0 & 0 & 0 \\
-1 & 2 & -1 & \cdots & 0 & 0 & 0 \\
0 & -1 & 2 & \cdots & 0 & 0 & 0 \\
\vdots & \vdots & \vdots & \ddots & \vdots & \vdots & \vdots \\
0 & 0 & 0 & \cdots & 2 & -1 & 0 \\
0 & 0 & 0 & \cdots & -1 & 2 & -1 \\
0 & 0 & 0 & \cdots & 0 & -1 & 2
\end{pmatrix}.
\tag{C4}
$$

The probability density in Eq. (3) is known if the matrix $\mathbf{c}$ is solved from the Lyapunov equation $\mathbf{a}\mathbf{c}^{-1} + \mathbf{c}^{-1}\mathbf{a}^{\mathrm{t}} = 2\mathbf{b}$, which gives

$$
\mathbf{c} = -\frac{2(g+M)}{M}
\begin{pmatrix}
2 & 1 & \cdots & 1 \\
1 & 2 & \cdots & 1 \\
\vdots & \vdots & \ddots & \vdots \\
1 & 1 & \cdots & 2
\end{pmatrix}
\tag{C5}
$$

for $M \geqslant 4$. The eigenvalues of the matrix $\begin{pmatrix} \cdot & \\ & \cdot \end{pmatrix}$ are M and 1 ($M-2$ degeneracy). Then all eigenvalues of $\mathbf{c}$ are negative (positive) if $g > -M$ ($g < -M$). It implies that the uNESS is thermodynamically stable (unstable) if $g > -M$ ($g < -M$).

To check the dynamical stability of the uNESS, we decompose $\mathbf{a}$ in Eq. (C3) into

$$
\mathbf{a} = -\frac{g+M}{4M}
\begin{pmatrix}
3 & 0 & 1 & 1 & \cdots & 1 & 1 & 1 \\
-1 & 2 & -1 & 0 & \cdots & 0 & 0 & 0 \\
0 & -1 & 2 & -1 & \cdots & 0 & 0 & 0 \\
0 & 0 & -1 & 2 & \cdots & 0 & 0 & 0 \\
\vdots & \vdots & \vdots & \vdots & \ddots & \vdots & \vdots & \vdots \\
0 & 0 & 0 & 0 & \cdots & 2 & -1 & 0 \\
0 & 0 & 0 & 0 & \cdots & -1 & 2 & -1 \\
1 & 1 & 1 & 1 & \cdots & 1 & 0 & 3
\end{pmatrix}
- \frac{p-q}{4}
\begin{pmatrix}
1 & 2 & 1 & 1 & \cdots & 1 & 1 & 1 \\
-1 & 0 & 1 & 0 & \cdots & 0 & 0 & 0 \\
0 & -1 & 0 & 1 & \cdots & 0 & 0 & 0 \\
0 & 0 & -1 & 0 & \cdots & 0 & 0 & 0 \\
\vdots & \vdots & \vdots & \vdots & \ddots & \vdots & \vdots & \vdots \\
0 & 0 & 0 & 0 & \cdots & 0 & 1 & 0 \\
0 & 0 & 0 & 0 & \cdots & -1 & 0 & 1 \\
-1 & -1 & -1 & -1 & \cdots & -1 & -2 & -1
\end{pmatrix}
$$

$$
\equiv -\frac{g+M}{4M}\mathbf{a}_g - \frac{p-q}{4}\mathbf{a}_p.
\tag{C6}
$$

By straightforward computation, it can be seen that all eigenvalues of $\mathbf{a}_g$ are real and positive, and that of $\mathbf{a}_p$ are purely imaginary. Note that $\mathbf{a}_g$ and $\mathbf{a}_p$ commute ($\mathbf{a}_g\mathbf{a}_p = \mathbf{a}_p\mathbf{a}_g$), implying that they share the same set of eigenvectors. Hence, the real part of the eigenvalues of $\mathbf{a}$ is equal to the eigenvalues of $-\frac{g+M}{4M}\mathbf{a}_g$. Then the real part of all eigenvalues of $\mathbf{a}$ are negative (positive) if $g > -M$ ($g < -M$). It implies that the uNESS is dynamically stable (unstable) if $g > -M$ ($g < -M$). Both the

dynamical and thermodynamic stability criteria are equivalent for the uNESS. This consequence is consistent with the theorem in Appendix B.

APPENDIX D: THERMODYNAMIC LAW

We are going to identify the thermodynamic law

$$\frac{dS}{dt} = \frac{d_i S}{dt} + \beta \frac{dE}{dt} + \beta \frac{dW}{dt} \tag{D1}$$

in the Ehrenfest urn ring model of arbitrary M.

The Boltzmann entropy of the system is given by

$$S = -\sum_{\vec{n}} \rho(\vec{n}, t) \ln \left(\rho(\vec{n}, t) / \frac{N!}{\prod_{i=1}^{M} n_i!} \right), \tag{D2}$$

where the multiplication factor $\frac{N!}{\prod_{i=1}^{M} n_i!}$ is due to the degeneracy of $\rho(\vec{n}, t)$. Applying Eq. (8), the entropy production rate becomes

$$\frac{dS}{dt} = -\sum_{\vec{n},\vec{m}} (W_{\vec{n},\vec{m}} \rho(\vec{m}, t)$$

$$- W_{\vec{m},\vec{n}} \rho(\vec{n}, t)) \ln \left(\rho(\vec{n}, t) / \frac{N!}{\prod_{i=1}^{M} n_i!} \right)$$

$$= \frac{N}{2} \sum_{\vec{n},\vec{m}} (W_{\vec{n},\vec{m}} \rho(\vec{m}, t)$$

$$- W_{\vec{m},\vec{n}} \rho(\vec{n}, t)) \ln \left(\frac{W_{\vec{n},\vec{m}} \rho(\vec{m}, t)}{W_{\vec{m},\vec{n}} \rho(\vec{n}, t)} \right)$$

$$+ \frac{N}{2} \sum_{\vec{n},\vec{m}} (W_{\vec{n},\vec{m}} \rho(\vec{m}, t)$$

$$- W_{\vec{m},\vec{n}} \rho(\vec{n}, t)) \ln \left(\frac{W_{\vec{m},\vec{n}} \frac{N!}{\prod_{i=1}^{M} n_i!}}{W_{\vec{n},\vec{m}} \frac{N!}{\prod_{i=1}^{M} m_i!}} \right)$$

$$= \frac{d_i S}{dt} + \frac{d_e S}{dt}, \tag{D3}$$

where the first term, $\frac{d_i S}{dt}$, is the internal entropy production rate [42], also known as Kullback-Leibler divergence [43]. By noting that

$$\frac{W_{\vec{m},\vec{n}}}{W_{\vec{n},\vec{m}}} = \frac{p}{q} \frac{n_i}{n_j + 1} e^{\frac{g}{N}(n_i - n_j - 1)}, \tag{D4}$$

if the jump is in anticlockwise (ac) direction, and in clockwise (c) direction,

$$\frac{W_{\vec{m},\vec{n}}}{W_{\vec{n},\vec{m}}} = \frac{q}{p} \frac{n_i}{n_j + 1} e^{\frac{g}{N}(n_i - n_j - 1)}. \tag{D5}$$

The second term, $\frac{d_e S}{dt}$, can be further rewritten as

$$\frac{d_e S}{dt} = \frac{N}{2} \sum_{\vec{n},\vec{m}} (W_{\vec{n},\vec{m}} \rho(\vec{m}, t) - W_{\vec{m},\vec{n}} \rho(\vec{n}, t)) \frac{g}{N}(n_i - n_j - 1)$$

$$+ \frac{N}{2} \sum_{\vec{n}} \sum_{\vec{m}}^{\text{ac}} (W_{\vec{n},\vec{m}} \rho(\vec{m}, t) - W_{\vec{m},\vec{n}} \rho(\vec{n}, t)) \ln \left(\frac{p}{q} \right)$$

$$+ \frac{N}{2} \sum_{\vec{n}} \sum_{\vec{m}}^{\text{c}} (W_{\vec{n},\vec{m}} \rho(\vec{m}, t) - W_{\vec{m},\vec{n}} \rho(\vec{n}, t)) \ln \left(\frac{q}{p} \right)$$

$$= \sum_{\vec{n},\vec{m}} g[n_j - (n_i - 1)] W_{\vec{m},\vec{n}} \rho(\vec{n}, t)$$

$$- N \ln \left(\frac{p}{q} \right) \sum_{\vec{n}} \sum_{\vec{m}}^{\text{ac}} (W_{\vec{m},\vec{n}} \rho(\vec{n}, t) - W_{\vec{n},\vec{m}} \rho(\vec{m}, t))$$

$$= \beta \frac{dE}{dt} + \beta \frac{dW}{dt}. \tag{D6}$$

The first term is the rate of change of energy and the second term is the rate of work done by the system, which can also be written as

$$\beta \frac{dW}{dt} = -\beta \mu \sum_{i=0}^{M-1} K_{i \to i+1}, \tag{D7}$$

where $\mu \equiv \beta^{-1} \ln(\frac{p}{q})$ is the effective chemical potential difference to actively drive the particle from one urn to another. $K_{i \to i+1}$ is the net particle flow from the ith to the $(i+1)$th urn, which is defined as

$$K_{i \to i+1} \equiv N \sum_{\vec{n}} \left(W_{(n_i-1, n_{i+1}+1),(n_i, n_{i+1})} - W_{(n_i+1, n_{i+1}-1),(n_i, n_{i+1})} \right) \rho(\vec{n}, t). \tag{D8}$$

Now the thermodynamic law in Eq. (D1) is identified. Note that it holds for the general thermodynamic (asymptotic and nonasymptotic states) process.

[1] C. W. Lynn, P. J. Cornblath, L. Papadopoulos, M. A. Bertolero, and D. S. Bassett, Proc. Natl. Acad. Sci. USA **23**, 118 (2021).

[2] K. Sekimoto, J. Phys. Soc. Jpn. **66**, 1234 (1997).

[3] U. Seifert, Phys. Rev. Lett. **95**, 040602 (2005).

[4] U. Seifert, Eur. Phys. J. B **64**, 423 (2008).

[5] U. Seifert, Rep. Prog. Phys. **75**, 126001 (2012).

[6] Y. Murashita and M. Esposito, Phys. Rev. E **94**, 062148 (2016).

[7] D. J. Evans, E. G. D. Cohen, and G. P. Morriss, Phys. Rev. Lett. **71**, 2401 (1993).

[8] G. Gallavotti and E. G. D. Cohen, Phys. Rev. Lett. **74**, 2694 (1995).

[9] J. Kurchan, J. Phys. A: Math. Gen. **31**, 3719 (1998).

[10] J. L. Lebowitz and H. Spohn, J. Stat. Phys. **95**, 333 (1999).

[11] C. Jarzynski, Phys. Rev. Lett. **78**, 2690 (1997).

[12] C. Jarzynski, Phys. Rev. E **56**, 5018 (1997).

[13] G. E. Crooks, Phys. Rev. E **60**, 2721 (1999).

[14] G. E. Crooks, Phys. Rev. E **61**, 2361 (2000).

[15] G. Hummer and A. Szabo, Proc. Natl Acad. Sci. USA **98**, 3658 (2001).

[16] T. Hatano and S. I. Sasa, Phys. Rev. Lett. **86**, 3463 (2001).

[17] Y. Oono and M. Paniconi, Prog. Theor. Phys. **130**, 29 (1998).

[18] S. I. Sasa and H. Tasaki, J. Stat. Phys. **125**, 125 (2006).

[19] M. Lax, Rev. Mod. Phys. **32**, 25 (1960).

[20] B. Derrida, Phys. Rep. **301**, 65 (1998).

[21] H. Qian, J. Phys. Chem. B **110**, 15063 (2006).

[22] M. Esposito, U. Harbola, and S. Mukamel, Rev. Mod. Phys. **81**, 1665 (2009).

[23] T. Herpich, J. Thingna, and M. Esposito, Phys. Rev. X **8**, 031056 (2018).

[24] T. Herpich and M. Esposito, Phys. Rev. E **99**, 022135 (2019).

[25] J. W. Ryu, A. Lazarescu, R. Marathe, and J. Thingna, New J. Phys. **23**, 105005 (2021).

[26] A. Lazarides, A. Das, and R. Moessner, Phys. Rev. Lett. **112**, 150401 (2014).

[27] K. Brandner and U. Seifert, Phys. Rev. E **93**, 062134 (2016).

[28] O. R. Diermann, H. Frerichs, and M. Holthaus, Phys. Rev. E **100**, 012102 (2019).

[29] H. J. Schmidt, J. Schnack, and M. Holthaus, Phys. Rev. E **100**, 042141 (2019).

[30] T. N. Ikeda and M. Sato, Sci. Adv. **6**, eabb4019 (2019).

[31] J. Liu, K. A. Jung, and D. Segal, Phys. Rev. Lett. **127**, 200602 (2021).

[32] J. Casado-Pascual, L. Lamata, and A. A. Reynoso, Phys. Rev. E **103**, 052139 (2021).

[33] C. H. Cheng, B. Gemao, and P. Y. Lai, Phys. Rev. E **101**, 012123 (2020).

[34] C. H. Cheng and P. Y. Lai, Phys. Rev. Res. **3**, 023134 (2021).

[35] H. Risken, *The Fokker-Planck Equation* (Springer, Berin, 1984).

[36] In equilibrium statistical mechanics, when N is large, this optimal point is usually called the saddle point. The partition function and any average physical variables are extended from a real to complex plane such that the optimal point in this complex plane is not locally maximum or minimum, but a saddle point. This saddle point in the complex plane corresponds to the fixed point in the parameter space of the Fokker-Planck equation. To avoid ambiguity to the readers, we avoid the terminology "saddle point" in the text.

[37] M. W. Hirsch, S. Smale, and R. L. Devaney, *Differential Equations, Dynamical Systems, and An Introduction to Chaos*, 2nd ed. (Elsevier, USA, 2004).

[38] C. H. Tseng, Y. M. Kao, and C. H. Cheng, Phys. Rev. E **96**, 032125 (2017).

[39] S. H. Strogatz, *Nonlinear Dynamics and Chaos: With Applications to Physics, Biology, Chemistry and Engineering*, 2nd ed. (CRC Press, New York, 2018).

[40] Quasistatic approximation in the text refers to the case that the dynamics of the slow variables [$\bar{\eta}(t)$ near the phase boundary] can be approximated by taking the time average of the fast oscillating terms in the equations.

[41] P. J. Antsaklis and A. N. Michel, *Linear Systems*, 2nd ed. (Birkhauser, Boston, 2006).

[42] J. Schnakenberg, Rev. Mod. Phys. **48**, 571 (1976).

[43] S. Kullback and R. A. Leibler, Ann. Math. Statist. **22**, 79 (1951).